*J. Fluid Mech.* (1995), *vol.* 290, *pp.* 345–376



# Modulation of three resonating gravity–capillary waves by a long gravity wave

By KARSTEN TRULSEN AND CHIANG C. MEI
Department of Civil and Environmental Engineering, Massachusetts Institute of Technology, Cambridge, MA 02139, USA

(Received 25 April 1994 and in revised form 18 November 1994)

We consider a resonant triad of gravity–capillary waves, riding on top of a much longer gravity wave. The long-wave phase is assumed to vary on the same scale as the slow modulation of the short waves. Envelope equations are first deduced in the Lagrangian description. By perturbation analysis for a weak long wave, we then find that the long wave can resonate the natural modulation oscillations of the triad envelope, giving rise to various bifurcations in the Poincaré map. Numerical integration for a stronger long wave reveals that chaos can emerge from these bifurcations. The bifurcation criterion of Chen & Saffman (1979) for collinear Wilton's ripples is generalized to arbitrary non-collinear triads, and is found to play an important role as a criterion for the onset of chaotic behaviour.

## 1. Introduction

In nature, gravity–capillary waves often appear in short-crested form. Our purpose here is to study the evolution of three resonating gravity–capillary waves propagating in different directions on the surface of a long gravity wave. This is important both for a fuller understanding of sea-surface dynamics and to facilitate interpretation of remote sensing data.

The theoretical study of resonant interactions between gravity–capillary waves was initiated by Harrison (1909) and Wilton (1915), who found that a progressive wave can excite its second harmonic through nonlinear interactions. The resulting waves are now known as Wilton's ripples. Extending the seminal work by Phillips (1960), who showed that pure gravity waves can resonate one another in quartets at the third order in wave steepness, McGoldrick (1965) showed that gravity–capillary waves can interact in triplets at the second order. He derived the nonlinear evolution equations under the assumption that the wave envelopes are uniform in space and subject to temporal modulation only, and found the analytical solution for waves modulated in amplitude, but not in phase. Simmons (1969) generalized the evolution equations to account for modulation of amplitude and phase, in time and space. Limiting to time evolution only, Simmons solved the quadratic evolution equations for three different waves in perfect resonance. Case & Chiu (1977) considered three-wave interaction where each wave consists of two components propagating in opposite directions. They found no coupling at the second order between the oppositely propagating waves. A general Hamiltonian account of triad resonance was given by Meiss & Watson (1978).

Bifurcations of uniform and steady wavetrains were studied by Chen & Saffman (1979). They showed that steady Wilton's ripples are associated with a period-doubling

bifurcation, through which a pure steady second harmonic wave can become a steady combination wave of the first and second harmonics. It was later shown independently by Reeder & Shinbrot (1981) and Ma (1982) that the same bifurcation can also occur for the special case of triad resonance in three dimensions when the two longer waves have the same amplitude and the wavenumber vectors form an isosceles triangle. Janssen (1986, 1987) showed that such period-doubling bifurcations may be facilitated by wind. Jones (1992) derived cubic nonlinear equations to investigate the modulational stability of Wilton's ripples of permanent form. Christodoulides & Dias (1994) considered the bifurcations of cubically nonlinear steady Wilton's ripples on the interface between two fluids of different densities.

The simultaneous evolution in time and space of the conservative three-wave equations has been solved analytically, see Kaup (1981) and references cited therein. For certain limiting cases, analytical solutions to the non-conservative three-wave equations are also known (Craik 1986). In general, non-conservative triad interaction can lead to chaos (Vyshkind & Rabinovich 1976; Wersinger, Finn & Ott 1980).

On the experimental side, collinear Wilton's ripples were verified by McGoldrick (1970). Banerjee & Korpel (1982) studied triads where the wavenumber vectors form an isosceles triangle. Recent experiments on more general configurations of triads have been described in a series of papers by Henderson & Hammack (1987), Perlin, Henderson & Hammack (1990) and Perlin & Hammack (1991), and surveyed by Henderson & Hammack (1993). They showed how a stability criterion of Hasselmann (1967), together with ubiquitous noise in their experiments, are important in the selection process that determines which discrete triads may emerge. Experiments on steep Wilton's ripples and higher-order harmonic resonances were performed by Perlin & Ting (1992), who compared the measured wave profiles with fully nonlinear theories and found good agreement. Field observations of three-wave resonant interactions under the influence of wind were reported by Strizhkin & Raletnev (1986).

Modern theories on the evolution of short waves on a long wave were begun by Longuet-Higgins & Stewart (1960), who discussed how the former steepen near the crests, and flatten near the troughs of the latter. Most of the existing works are concerned with the linear evolution of a single train of gravity or gravity–capillary waves, over a relatively short time or distance which is comparable with a long-wave period or wavelength. Phillips (1981) studied the evolution of a short linear gravity–capillary wave on a prescribed long wave, in an orthogonal coordinate system defined by the long-wave surface. Longuet-Higgins (1987) considered the effects of a steep long wave which was calculated numerically. The linear evolution of gravity–capillary waves on steep gravity waves was considered by Grimshaw (1988) by using non-orthogonal curvilinear coordinates. A Zhakharov spectral formulation for long-wave/short-wave interaction was presented by Craik (1988). A general Hamiltonian account of the linear evolution of short waves on a long wave was given by Henyey *et al.* (1988). Shyu & Phillips (1990) investigated the possibility of blocking of short waves by the variable orbital velocity of a long wave.

The nonlinear evolution of a short gravity wave on a long gravity wave was investigated by Zhang & Melville (1990) by using an orthogonal curvilinear coordinate system. Subsequently, Zhang & Melville (1992) used this theory to investigate the evolution of a narrow-banded wavetrain on top of a long wave. Naciri & Mei (1992) used a Lagrangian formulation through which a short gravity wave was described relative to the long-wave particle displacement. They let the long wave be a rotational Gerstner wave of finite slope. It was found that the long wave enlarges the domain of Benjamin–Feir instability in the parametric space. Naciri & Mei (1992) further found

that the post-instability evolution is chaotic, therefore suggesting that the irregular appearance of the sea surface need not be solely due to the turbulent eddies in wind, but is inherent in the deterministic nonlinear mechanics of the water surface. Woodruff & Messiter (1994) recently derived a theory for short capillary waves riding on a long gravity wave of finite steepness.

In this paper, we are interested in the long-time evolution of short surface waves. For a meaningful theoretical analysis it is important to assess the role of viscous damping. Let us first show that for a fresh and clean surface without the effects of aging or contamination, viscous damping occurs over a timescale much longer than the time for quadratic interaction. At 20°C the following values for surface tension, density, gravitational acceleration and viscosity can be taken:

$$T = 72.8\times10^{-3}\ \mathrm{N\,m^{-1}},\quad \rho = 9.98\times10^{2}\ \mathrm{kg\,m^{-3}},\quad g = 9.80\ \mathrm{m\,s^{-2}},\quad \nu = 1.00\times10^{-6}\ \mathrm{m^2\,s^{-1}}.$$

We define the characteristic wavenumber and frequency by equating the gravity and capillary terms in the dispersion relation, i.e.

$$k^* = \left(\frac{\rho g}{T}\right)^{1/2} = 367\ \mathrm{m^{-1}} = \frac{2\pi}{1.7\ \mathrm{cm}},\qquad \omega^* = (2gk^*)^{1/2} = 84.8\ \mathrm{s^{-1}} = 2\pi\times 13\ \mathrm{Hz}. \tag{1.1}$$

For a clean water surface, the ratio of a wave period to the damping time is

$$\frac{1}{\omega^*}2\nu(k^*)^2 = 0.0032.$$

The ratio of a wave period to the timescale of resonant interaction is comparable to the wave steepness. If we let the steepness be of order $\epsilon = O(0.05)$–$O(0.1)$, then viscous damping is clearly unimportant for a time range compatible with quadratic nonlinear interaction. Hence damping will be ignored in this study even for the examination of the long-time effect of nonlinearity. However, it is equally clear that viscous effects cannot be neglected for a cubically nonlinear theory. If on the other hand contamination is so strong that the surface behaves as an inextensible film, the non-dimensional characteristic damping rate can be found to be

$$\frac{1}{\omega^*}\frac{k^*}{2}\left(\frac{\nu\omega^*}{2}\right)^{1/2} = 0.014.$$

Viscosity would then be much more important in the study of the long-time behaviour. Based on these estimates, we shall here assume that the water surface is clean, and consider inviscid triad interaction up to quadratic nonlinear order, with the effect of the long wave balanced at the second order.

Assuming that the amplitude of the long wave is much greater than the typical wavelength of the short waves, we employ in §2 the Lagrangian description (Naciri & Mei 1992) in order to simplify the consideration of the free surface. Multiple-scales perturbation expansions are introduced in §3. Equations for the envelopes of the interacting short waves on top of a uniform long wave are deduced in §4. The reduced dynamical system for time evolution is introduced in §5. To facilitate the discussion of the influence of the long wave, we first summarize the well-known analytical solution for a resonant triad without a long wave in §6. As a result, we generalize the bifurcation criterion of Chen & Saffman (1979), Reeder & Shinbrot (1981) and Ma (1982) to arbitrary three-wave configurations. For a weak long wave, approximate analysis is then pursued in §7 to reveal bifurcations due to modulational resonance, by which the natural envelope oscillations of the triad are resonated by

the long wave. Confirmation of the analytical results by direct numerical integration of the evolution equations, is also shown. Finally, numerical results for a relatively strong long wave are presented in §8. Details of the approach to Hamiltonian chaos are shown.

## 2. Governing Lagrangian equations

We adopt the Lagrangian coordinates in Naciri & Mei (1992) and first summarize the equations governing irrotational deep-water waves on the surface of an inviscid, incompressible fluid. The instantaneous horizontal and vertical position of a fluid particle, $\boldsymbol{X} = (X, Y)$ and $Z$ is parameterized by the reference coordinates $\boldsymbol{a} = (a, b)$ and $c$ and time $t$. Continuity of an incompressible fluid requires that the following Jacobian is independent of time:

$$J(\boldsymbol{a}, c, t) \equiv \frac{\partial(\boldsymbol{X}, Z)}{\partial(\boldsymbol{a}, c)} = J(\boldsymbol{a}, c, 0). \tag{2.1}$$

The vorticity components are required to be zero,

$$\boldsymbol{\Omega}_X = (\Omega_X, \Omega_Y) = \boldsymbol{0}, \qquad \Omega_Z = 0. \tag{2.2a,b}$$

For deep water waves, irrotationality in the two horizontal directions implies irrotationality in the vertical direction. This follows from the vector identity $\nabla \cdot \nabla \times \boldsymbol{v} = 0$. If $\boldsymbol{\Omega}_X = \boldsymbol{0}$, then $\Omega_Z$ is independent of $Z$. Since the fluid velocity $\boldsymbol{v}$ vanishes at great depth ($Z \to -\infty$), it follows that $\Omega_Z$ vanishes everywhere. As a result, (2.1) and (2.2$a$) are sufficient to determine the three unknowns $X, Y, Z$.

On the free surface, designated by $c = 0$, we have

$$\nabla_a X \frac{\partial^2 X}{\partial t^2} + \nabla_a Y \frac{\partial^2 Y}{\partial t^2} + \nabla_a Z \left( \frac{\partial^2 Z}{\partial t^2} + g \right) = -\frac{1}{\rho} \nabla_a p, \tag{2.3}$$

where $p$ is the water pressure, $\rho$ the water density, $g$ the acceleration due to gravity and $\nabla_a = (\partial/\partial a, \partial/\partial b)$. In terms of the vertical displacement of the free surface $\zeta = Z(\boldsymbol{a}, 0, t)$, the water pressure at the free surface is given by

$$p = p_{\text{atm}} + T \nabla_X \cdot \frac{(-\nabla_X \zeta, 1)}{(1 + |\nabla_X \zeta|^2)^{1/2}}. \tag{2.4}$$

Here $p_{\text{atm}}$ is the atmospheric pressure, $T$ the surface tension between water and air and $\nabla_X = (\partial/\partial X, \partial/\partial Y)$. The atmospheric pressure is taken to be constant,

$$\nabla_a p_{\text{atm}} = \boldsymbol{0} \quad \text{at} \quad c = 0. \tag{2.5}$$

In the following, we set $\gamma = T/\rho$.

It is convenient to introduce the Lagrangian displacements $\boldsymbol{x} = (x, y)$ and $z$ relative to the reference coordinates $(\boldsymbol{a}, c)$ as follows:

$$\boldsymbol{X} = \boldsymbol{a} + \boldsymbol{x}(\boldsymbol{a}, c, t), \qquad Z = c + z(\boldsymbol{a}, c, t). \tag{2.6}$$

In summary, the unknown displacements $x, y, z$ can be solved from the continuity condition (2.1) and the irrotationality condition (2.2$a$), subject to the dynamic boundary condition (2.3)–(2.5). The resulting equations in terms of $x, y, z$ are lengthy, and are given in the Appendix.

## 3. Order assumptions and multiple-scale expansions

We shall assume that the water depth is much greater than the length of the long wave and that both short and long waves have small steepnesses. Let the physical wavenumber, frequency and amplitude of the short wave be denoted by $k, \omega, A$, respectively, and the corresponding quantities for the long wave by $K, \Omega, B$. The following ordering assumptions are assumed with a view to yielding simple and interesting asymptotic results:

$$kA = O(\epsilon), \qquad KB = O(\epsilon), \qquad K/k = O(\epsilon^2), \qquad \Omega/\omega = O(\epsilon), \tag{3.1}$$

where $\epsilon \ll 1$. The last two are dictated by the anticipated dispersion relations

$$\Omega^2 = gK \quad \text{and} \quad \omega^2 = gk + \gamma k^3. \tag{3.2a,b}$$

Under these scaling assumptions,

$$\Omega B = O(\omega/k) \quad \text{and} \quad kB = O(1/\epsilon), \tag{3.3}$$

meaning, respectively, that the orbital velocity of the long wave is comparable in order of magnitude to the phase and group velocities of the short waves, and that the short wavelength is much smaller than the long-wave amplitude.

We assume that the long wave propagates in the $x$-direction, while the resonating short waves propagate in any horizontal direction. As a consequence, the long wave will have only $x$ and $z$ components, which are independent of the reference coordinate $b$.

We let the basic reference lengthscales and timescales be defined by $k^{-1}$ and $\omega^{-1}$ of the short wave. In view of the scale contrast between short and long waves and the anticipated growth due to resonance, we introduce a cascade of slow coordinates

$$(\boldsymbol{a}_j, c_j, t_j) = \epsilon^j(\boldsymbol{a}, c, t) \quad \text{for} \quad j = 1, 2, 3, \ldots \tag{3.4}$$

where $\boldsymbol{a}_j = (a_j, b_j)$. From (3.1) the amplitudes of the short and long waves are $O(\epsilon/k)$ and $O(1/\epsilon k)$ respectively, and hence the particle displacement field can to the leading order be decomposed into long-wave components at $O(\epsilon^{-1})$, and short-wave components at $O(\epsilon)$. The lowest order at which the short waves can influence the long wave is $O(KB(kA)^2)$. On the other hand, triad resonance of short waves is known to reach maturity at $O(kA)^2$ over the timescale $t_1 = O(1)$. Self-modulation of the long wave will occur by nonlinear interaction at the third order over the much longer time and length scales $a_3, c_3, t_2$. The short waves will be modulated by both nonlinear self-interaction and by the long wave. Self-interaction must be described by coordinates $\boldsymbol{a}_1, c_1, t_1$. Modulation of the short waves by the long wave will of course be over the scales of the long wave.

In this paper we shall only examine the effect of a long wave on the second-order interactions of the short waves, over the timescale of triad resonance $t_1$. Hence the long wave will not be affected by the short waves and can be described by a linearized theory. Thus we expand the short-wave displacements to the second order, while we only need the long-wave displacement to the leading order. The resulting expansions, with both long and short-wave contributions are

$$\left.\begin{aligned} x &= \epsilon^{-1}x^{(-1)} + \epsilon x^{(1)} + \epsilon^2 x^{(2)}, \\ y &= \qquad\quad \epsilon y^{(1)} + \epsilon^2 y^{(2)}, \\ z &= \epsilon^{-1}z^{(-1)} + \epsilon z^{(1)} + \epsilon^2 z^{(2)}. \end{aligned}\right\} \tag{3.5}$$

The long-wave contributions at $O(\epsilon^{-1})$ depend on $a_2, c_2, t_1$. The short-wave contributions at $O(\epsilon)$ and $O(\epsilon^2)$ depend on $\boldsymbol{a}, \boldsymbol{a}_1, c, c_1, t, t_1$.

The leading-order equations for the long wave are
continuity:

$$\frac{\partial x^{(-1)}}{\partial a_2} + \frac{\partial z^{(-1)}}{\partial c_2} = 0, \tag{3.6}$$

irrotationality:

$$\frac{\partial^2 x^{(-1)}}{\partial c_2 \partial t_1} - \frac{\partial^2 z^{(-1)}}{\partial a_2 \partial t_1} = 0, \tag{3.7}$$

free surface condition:

$$\frac{\partial^2 x^{(-1)}}{\partial t_1^2} + g \frac{\partial z^{(-1)}}{\partial a_2} = 0. \tag{3.8}$$

These equations are satisfied by the basic linear wave solution

$$x^{(-1)} = x^{(-1,0)} + \frac{\mathrm{i}}{2} B \mathrm{e}^{\mathrm{i}(Ka_2 - \Omega t_1) + Kc_2} + \text{c.c.}, \tag{3.9a}$$

$$z^{(-1)} = z^{(-1,0)} + \tfrac{1}{2} B \mathrm{e}^{\mathrm{i}(Ka_2 - \Omega t_1) + Kc_2} + \text{c.c.}, \tag{3.9b}$$

where $B$ is the long-wave amplitude and $\Omega$ and $K$ are related by the dispersion relation (3.2*a*), and c.c. denotes complex conjugate. The Stokes drift of the long wave $(x^{(-1,0)}, z^{(-1,0)})$ is not needed in the subsequent analysis.

The first- and second-order equations for the short waves, corresponding to $m = 1$ and $m = 2$, respectively, are
continuity:

$$\nabla_a \cdot \boldsymbol{x}^{(m)} + \frac{\partial z^{(m)}}{\partial c} = \mathscr{E}^{(m)}, \tag{3.10}$$

irrotationality:

$$\frac{\partial^2 \boldsymbol{x}^{(m)}}{\partial c \partial t} - \nabla_a \frac{\partial z^{(m)}}{\partial t} = (\mathscr{G}^{(m)}, \mathscr{F}^{(m)}), \tag{3.11}$$

free surface condition:

$$\frac{\partial^2 \boldsymbol{x}^{(m)}}{\partial t^2} + g \nabla_a z^{(m)} - \gamma \nabla_a^2 \nabla_a z^{(m)} = (\mathscr{H}^{(m)}, \mathscr{I}^{(m)}). \tag{3.12}$$

The right-hand sides of (3.11) and (3.12) give the two components of the vectors which depend on lower-order solutions. The leading-order short-wave problem is homogeneous, with $\mathscr{E}^{(1)} = \mathscr{F}^{(1)} = \mathscr{G}^{(1)} = \mathscr{H}^{(1)} = \mathscr{I}^{(1)} = 0$. The lengthy right-hand-side expressions of the second-order problem, $\mathscr{E}^{(2)}$, $\mathscr{F}^{(2)}$, $\mathscr{G}^{(2)}$, $\mathscr{H}^{(2)}$ and $\mathscr{I}^{(2)}$, have been derived by the symbolic computation program MACSYMA, but are not given here.

## 4. Evolution equations for the short waves

Let us begin with three trains of short waves with amplitudes $A_n$ for $n = 1, 2, 3$. The leading-order sum of the short waves is given by

$$\boldsymbol{x}^{(1)} = \boldsymbol{x}^{(1,0)} + \frac{\mathrm{i}}{2} \sum_{n=1}^{3} \frac{\boldsymbol{k}_n}{k_n} A_n \mathrm{e}^{\mathrm{i}\theta_n + k_n c} + \text{c.c.}, \tag{4.1a}$$

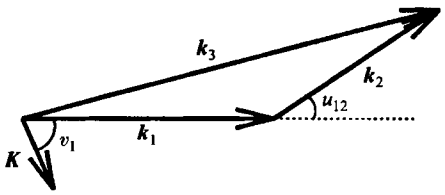


FIGURE 1. Geometry of a resonating triad. The angle $v_n$ is between the long wave $\boldsymbol{K}$ and the short wave $\boldsymbol{k}_n$. The angle $u_{12}$ is between the short waves $\boldsymbol{k}_1$ and $\boldsymbol{k}_2$. The short wave $\boldsymbol{k}_3$ is always the shortest one.

$$z^{(1)} = z^{(1,0)} + \frac{1}{2}\sum_{n=1}^{3} A_n e^{i\theta_n + k_n c} + \text{c.c.} \tag{4.1b}$$

The wavenumber vector of the $n$th wave is $\boldsymbol{k}_n = (k_{a,n}, k_{b,n})$ with $k_n = |\boldsymbol{k}_n|$, while the phase is $\theta_n = \boldsymbol{k}_n \cdot \boldsymbol{a} - \omega_n t$. Each amplitude $A_n(\boldsymbol{a}_1, c_1, t_1)$ depends on the slow coordinates only. Upon substitution of (4.1) into the leading-order equations (3.10)–(3.12), we get the dispersion relation for each short wave from the first-harmonic problem

$$\omega_n^2 = gk_n + \gamma k_n^3. \tag{4.2}$$

Note that Doppler's effect is not apparent in the Lagrangian dispersion relation. This is because the Lagrangian representation describes the short waves relative to fluid particles that move with the long wave. The short waves are hence described in an accelerated reference system such that they do not appear to be advected by the long wave. By transformation to a stationary Eulerian coordinate system, it can be shown that the Lagrangian dispersion relation (4.2) contains implicitly the anticipated Doppler shift due to the long wave.

The Stokes drift due to the short waves $(\boldsymbol{x}^{(1,0)}, z^{(1,0)})$ can be solved from the zeroth-harmonic problem, but is not needed here.

The evolution equations for three resonant short waves are found at the second order. First the resonance conditions must be satisfied

$$\left.\begin{aligned} \boldsymbol{k}_3 &= \boldsymbol{k}_1 + \boldsymbol{k}_2 \\ \omega_3 &= \omega_1 + \omega_2 \end{aligned}\right\} \Rightarrow \theta_3 = \theta_1 + \theta_2, \tag{4.3}$$

where each individual wave satisfies the dispersion relation (4.2).

Figure 1 shows a typical geometry of a resonating triad, with wavenumber vectors $\boldsymbol{k}_1$, $\boldsymbol{k}_2$ and $\boldsymbol{k}_3$. The angle between vectors $\boldsymbol{k}_1$ and $\boldsymbol{k}_2$ is denoted by $u_{12}$, as indicated in the figure. This angle is always less than 90° (see footnote in McGoldrick 1965, p. 309). We therefore denote $\boldsymbol{k}_3$ the shortest wave, and $\boldsymbol{k}_1$ and $\boldsymbol{k}_2$ the two longer waves.

The second-order solution is assumed to be of the form

$$\boldsymbol{x}^{(2)} = \boldsymbol{x}^{(2,0)} + \frac{\mathrm{i}}{2}\sum_{n=1}^{3} \frac{\boldsymbol{k}_n}{k_n}\left(\boldsymbol{x}_n^{(2,1)} e^{i\theta_n} + \boldsymbol{x}_n^{(2,2)} e^{2i\theta_n}\right) + \text{c.c.}, \tag{4.4a}$$

$$z^{(2)} = z^{(2,0)} + \frac{1}{2}\sum_{n=1}^{3}\left(z_n^{(2,1)} e^{i\theta_n} + z_n^{(2,2)} e^{2i\theta_n}\right) + \text{c.c.} \tag{4.4b}$$

The zeroth harmonics $(\boldsymbol{x}^{(2,0)}, z^{(2,0)})$ are corrections to the Stokes drift, while $(\boldsymbol{x}_n^{(2,1)}, z_n^{(2,1)})$ and $(\boldsymbol{x}_n^{(2,2)}, z_n^{(2,2)})$ are the slowly varying amplitudes of the first and second harmonics, each of which depends on the scales $(\boldsymbol{a}_1, c, c_1, t_1)$. We only need to consider the

first-harmonic displacements. The problem then becomes

$$\frac{\partial z_n^{(2,1)}}{\partial c} - \frac{k_{a,n}^2}{k_n} x_n^{(2,1)} - \frac{k_{b,n}^2}{k_n} y_n^{(2,1)} = E_n, \tag{4.5}$$

$$\frac{\partial y_n^{(2,1)}}{\partial c} - k_n z_n^{(2,1)} = F_n, \qquad \frac{\partial x_n^{(2,1)}}{\partial c} - k_n z_n^{(2,1)} = G_n \tag{4.6}$$

with surface boundary conditions

$$z_n^{(2,1)} - x_n^{(2,1)} = H_n, \qquad z_n^{(2,1)} - y_n^{(2,1)} = I_n \qquad \text{at} \quad c = 0. \tag{4.7}$$

By using MACSYMA, the lengthy expressions $E_n$, $F_n$, $G_n$, $H_n$ and $I_n$ have been obtained, but are not reproduced here. The above inhomogeneous differential system possesses non-trivial homogeneous solutions and must be subjected to the following solvability condition for each $n$:

$$\int_{-\infty}^{0} e^{k_n c}(k_n^2 E_n - k_{a,n}^2 G_n - k_{b,n}^2 F_n)\,dc = k_{a,n}^2 H_n + k_{b,n}^2 I_n \qquad \text{for} \quad n = 1, 2, 3. \tag{4.8}$$

As results of solvability, the evolution equations for the envelopes of the three resonating short waves riding on the long wave are obtained:

$$\frac{\partial A_1}{\partial t_1} + \boldsymbol{c}_{g,1} \cdot \nabla_{a_1} A_1 + i\beta_1 A_1 \cos\phi + i\alpha_1 A_2^* A_3 = 0, \tag{4.9a}$$

$$\frac{\partial A_2}{\partial t_1} + \boldsymbol{c}_{g,2} \cdot \nabla_{a_1} A_2 + i\beta_2 A_2 \cos\phi + i\alpha_2 A_1^* A_3 = 0, \tag{4.9b}$$

$$\frac{\partial A_3}{\partial t_1} + \boldsymbol{c}_{g,3} \cdot \nabla_{a_1} A_3 + i\beta_3 A_3 \cos\phi + i\alpha_3 A_1 A_2 = 0. \tag{4.9c}$$

Here, $\boldsymbol{c}_{g,n}$ is the group velocity

$$\boldsymbol{c}_{g,n} = \frac{g + 3\gamma k_n^2}{2\omega_n} \frac{\boldsymbol{k}_n}{k_n}, \tag{4.10}$$

and $\nabla_{a_1} = (\partial/\partial a_1, \partial/\partial b_1)$. The coefficients for nonlinear interaction between short waves are

$$\alpha_n = \frac{k_n}{\omega_n}\alpha, \qquad n = 1, 2, 3, \tag{4.11}$$

where

$$\begin{aligned} 16k_1k_2k_3\alpha &= g\,(k_3 - k_2 - k_1)(k_3 - k_2 + k_1)(k_3 + k_2 - k_1)(k_3 + k_2 + k_1) \\ &+ \gamma\left\{(k_1 + k_2 + k_3)^2\left[k_1^3(k_1 - k_2 - k_3) + k_2^3(k_2 - k_1 - k_3) + k_3^3(k_3 - k_1 - k_2)\right]\right. \\ &\left. + 4k_1k_2k_3\left[k_1^2(k_2 + k_3) + k_2^2(k_1 + k_3) + k_3^2(k_1 + k_2)\right]\right\}. \end{aligned} \tag{4.12}$$

Our nonlinear coefficients are equal to those of McGoldrick (1965) (after correcting a typographical error), Simmons (1969) and Case & Chiu (1977), all derived in the Eulerian frame.

The long-wave phase is

$$\phi = Ka_2 - \Omega t_1 + \arg B, \tag{4.13}$$

and the long-wave/short-wave interaction coefficients are

$$\beta_n = \left\{\frac{3\omega_n^2 K - 2k_n\Omega^2}{2\omega_n}\cos^2 v_n - \frac{\Omega^2 k_n}{2\omega_n}\right\}|B| \tag{4.14a}$$

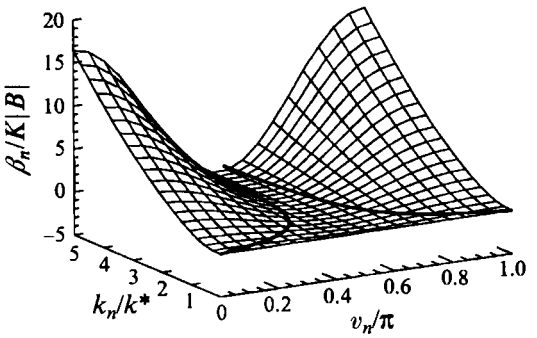


FIGURE 2. The long-wave/short-wave interaction coefficient $\beta_n/KB$ as a function of the angle $v_n/\pi$ and the wavenumber $k_n/k^*$. The zero crossings are indicated by thick contour lines.

$$= K|B|\frac{k_n}{2\omega_n}\left(3\gamma k_n^2\cos^2 v_n - g\sin^2 v_n\right). \tag{4.14b}$$

Here, the angle between the long and the short wavenumber vectors $\boldsymbol{K}$ and $\boldsymbol{k}_n$ is denoted by $v_n$ (see figure 1).

Physically, the first term in (4.14*a*) is due to the long-wave-induced horizontal acceleration of the Lagrangian coordinates. This term would be absent in a stationary Eulerian description (e.g. Grimshaw 1988), but would be present in a horizontally accelerated system such that the short waves appear to propagate in a stationary medium. The presence of this interaction is therefore associated with the fact that the Lagrangian dispersion relation for the short waves does not explicitly show a Doppler shift.

The last term in (4.14*a*) accounts for the vertical acceleration of the long-wave surface, and gives a modification to the effective gravitational acceleration felt by the short waves as they ride on top of the long wave. In some works on long-wave/short-wave interaction (e.g. Grimshaw 1988) this modification is accounted for in the dispersion relation for the short wave, and does not appear as part of the interaction coefficient between the long and the short waves.

It is important to note that under the assumed scale ratios, the Lagrangian spatial gradients involve $\boldsymbol{a}_1$ only, but not $\boldsymbol{a}_2$. Within the domain defined by $O(t_1) = 1$ and $O(\boldsymbol{a}_1) = 1$, the spatial dependence of the long wave is only of parametric significance; only the time dependence matters. Thus the direct effect of the long wave is that of a time-periodic, but spatially uniform flow.

Each of the coefficients $\beta_n$ is strictly positive if the short and the long waves are collinear, and strictly negative if they are orthogonal. A typical $\beta_n$ vanishes for some intermediate angle of incidence $\bar{v}_n$ independent of the long wave,

$$\tan^2\bar{v}_n = \frac{3\gamma k_n^2}{g}. \tag{4.15}$$

Figure 2 shows the variation of $\beta_n/KB$ as a function of the short-wave wavenumber $k_n/k^*$ and the angle $v_n$ between the short wave and the long wave. The zero crossings of $\beta_n$ are plotted as thick contour curves on the surface.

We remark that in the absence of nonlinear interactions, our coefficient $\beta_n$ can only affect the phase and not the amplitude of a single linear short wave. In a resonating triad, however, the phases of any two waves will affect the amplitude of the third wave through the nonlinear interaction terms. Our long-wave/short-wave interaction

coefficients are therefore sufficient to describe both amplitude and phase modulation of the waves in a triad.

Because the interaction coefficients $\beta_n$ are multiplied by the imaginary unit, the long wave cannot affect the total energy or linear momentum of the resonating short waves. Exchange of energy, momentum and action takes place only among the short waves, and not between the short waves and the long wave.

## 5. Dynamical system for time evolution

The system of partial differential equations (4.9) is difficult to analyse. We shall restrict our consideration to the special case where the evolution is uniform in the spatial modulation coordinates $\boldsymbol{a}_1$. Since the particle displacement is dominated by the long-wave motion, the coordinate $\boldsymbol{a} = \boldsymbol{X} - \epsilon^{-1}\boldsymbol{x}_{-1} + O(\epsilon)$ is essentially drifting with fluid particles moved by the long wave. Thus $\nabla_{\boldsymbol{a}_1} = \boldsymbol{0}$ means that in this accelerated coordinate system, the short waves are not modulated in space.

However, we shall allow for a small detuning from resonance. Detuning can be considered as a special type of slow space modulation. Let $(\boldsymbol{k}_n, \omega_n)$ describe the short waves in perfect resonance,

$$\boldsymbol{k}_1 + \boldsymbol{k}_2 - \boldsymbol{k}_3 = \boldsymbol{0}, \quad \omega_1 + \omega_2 - \omega_3 = 0, \quad \omega_n = \omega(\boldsymbol{k}_n), \tag{5.1a,b,c}$$

while $\boldsymbol{k}'_n$ describes the detuned short-wavenumber vectors

$$\boldsymbol{k}'_n = \boldsymbol{k}_n + \epsilon\boldsymbol{\delta}_n. \tag{5.2}$$

Detuning can be expressed as envelope modulation by the following substitution:

$$A_n = \bar{A}_n e^{i\boldsymbol{\delta}_n \cdot \boldsymbol{a}_1}, \qquad n = 1, 2, 3, \tag{5.3}$$

where the short-wave field $(\bar{A}_n)$ is uniform with respect to $\boldsymbol{a}_1$. For consistency, it is then necessary to assume that the detuned wavenumbers satisfy the resonance condition (5.1$a$) exactly, hence

$$\boldsymbol{\delta}_1 + \boldsymbol{\delta}_2 - \boldsymbol{\delta}_3 = \boldsymbol{0}. \tag{5.4}$$

In the following, it is convenient to employ the normalized variables

$$t = -\phi = -(Ka_2 - \Omega t_1 + \arg B), \tag{5.5}$$

$$A'_n = \left(\frac{\omega_n}{k_n}\right)^{1/2} \bar{A}_n, \qquad \beta'_n = \frac{\beta_n}{\Omega}, \qquad \alpha' = \frac{2\alpha}{\Omega}\left(\frac{k_1 k_2 k_3}{\omega_1 \omega_2 \omega_3}\right)^{1/2}, \qquad \Delta'_n = \frac{\boldsymbol{c}_{g,n} \cdot \boldsymbol{\delta}_n}{\Omega}. \tag{5.6}$$

The evolution equations then become

$$\frac{dA'_1}{dt} = -i\frac{\alpha'}{2} A'^*_2 A'_3 - i\beta'_1 A'_1 \cos t - i\Delta'_1 A'_1, \tag{5.7a}$$

$$\frac{dA'_2}{dt} = -i\frac{\alpha'}{2} A'^*_1 A'_3 - i\beta'_2 A'_2 \cos t - i\Delta'_2 A'_2, \tag{5.7b}$$

$$\frac{dA'_3}{dt} = -i\frac{\alpha'}{2} A'_1 A'_2 - i\beta'_3 A'_3 \cos t - i\Delta'_3 A'_3. \tag{5.7c}$$

We now introduce polar coordinates $A'_n = I_n^{1/2} e^{i\theta_n}$ where $I_n \geqslant 0$. In physical variables, $I_n = (\omega_n/k_n)|A_n|^2$ is proportional to the wave action of the $n$th short wave. After separating the real and imaginary parts, we get a system of six real equations:

$$\frac{dI_1}{dt} = \frac{dI_2}{dt} = -\frac{dI_3}{dt} = -\alpha'(I_1 I_2 I_3)^{1/2} \sin(\theta_1 + \theta_2 - \theta_3), \tag{5.8}$$

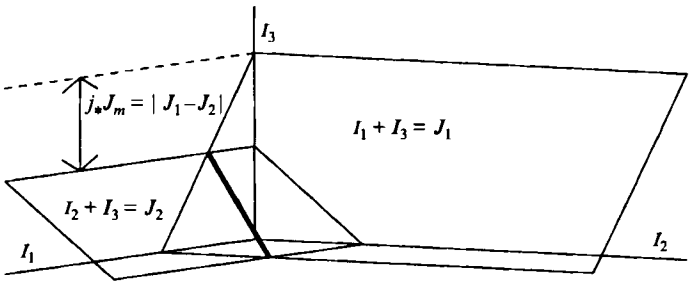


FIGURE 3. Intersection between two planes. The axes represent the wave actions of individual short waves. The action conservation laws are indicated as planes. The exchange of action between the three resonating waves must happen along the line of intersection. The difference between the actions of the longer waves is indicated by $j_*$.

$$\frac{\mathrm{d}\theta_1}{\mathrm{d}t} = -\frac{\alpha'}{2}\left(\frac{I_2 I_3}{I_1}\right)^{1/2}\cos(\theta_1+\theta_2-\theta_3) - \beta_1'\cos t - \Delta_1', \tag{5.9a}$$

$$\frac{\mathrm{d}\theta_2}{\mathrm{d}t} = -\frac{\alpha'}{2}\left(\frac{I_1 I_3}{I_2}\right)^{1/2}\cos(\theta_1+\theta_2-\theta_3) - \beta_2'\cos t - \Delta_2', \tag{5.9b}$$

$$\frac{\mathrm{d}\theta_3}{\mathrm{d}t} = -\frac{\alpha'}{2}\left(\frac{I_1 I_2}{I_3}\right)^{1/2}\cos(\theta_1+\theta_2-\theta_3) - \beta_3'\cos t - \Delta_3'. \tag{5.9c}$$

The dimension of this dynamical system can be reduced from six to four by using the conserved quantities $I_1 + I_3$ and $I_2 + I_3$. Let

$$\begin{pmatrix}\psi\\ \beta\\ \Delta\end{pmatrix} = \begin{pmatrix}\theta_1+\theta_2-\theta_3\\ \beta_3'-\beta_2'-\beta_1'\\ \Delta_3'-\Delta_2'-\Delta_1'\end{pmatrix} \quad \text{and} \quad \begin{pmatrix}J\\ J_1\\ J_2\end{pmatrix} = \begin{pmatrix}I_3\\ I_1+I_3\\ I_2+I_3\end{pmatrix}, \tag{5.10}$$

where $J$ is proportional to the wave action of the shortest wave. The new equations for $J$ and $\psi$ are

$$\frac{\mathrm{d}J}{\mathrm{d}t} = \alpha'\,[J(J_1-J)(J_2-J)]^{1/2}\sin\psi, \tag{5.11a}$$

$$\frac{\mathrm{d}\psi}{\mathrm{d}t} = -\alpha'\frac{-3J^2+2(J_1+J_2)J-J_1J_2}{2\,[J(J_1-J)(J_2-J)]^{1/2}}\cos\psi + \Delta + \beta\cos t. \tag{5.11b}$$

The phase angles $\theta_1$ and $\theta_2$ are decoupled from these, and can be found from (5.9*b*) and (5.9*c*). Thus we have in fact reduced the original set of six real equations to a dynamical system for two variables $J$ and $\psi$.

If $I_1$, $I_2$ and $I_3$ are used to form a rectilinear coordinate system, the conserved quantities $J_1$ and $J_2$ define two planes. The line of intersection between the two planes defines the range of $J$. Since $I_n \geqslant 0$, only the segment extending from $J = 0$ to $J = \min\{J_1, J_2\}$ is physically meaningful, as sketched in figure 3. All exchange of action between the short waves is confined to this line segment. The line can be parameterized by $0 \leqslant j \leqslant 1$ where

$$J = J_m(1-j) \qquad \text{and} \qquad J_m = \min\{J_1, J_2\}. \tag{5.12}$$

Hence $j = 1$ corresponds to $I_3 = 0$, $j = 0$ corresponds to the maximum $I_3$, and $(1-j)$ is a measure of the action of the shortest wave.

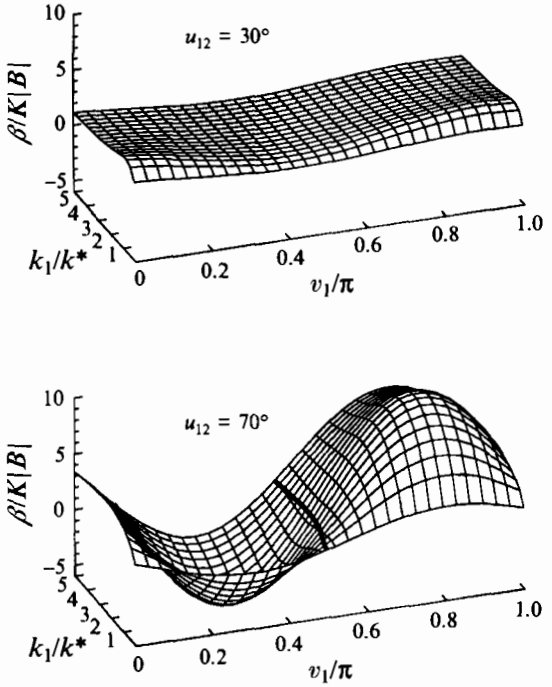


FIGURE 4. The effective long-wave/short-wave interaction coefficient $\beta/K|B|$ as a function of the angle of incidence $v_1/\pi$ and the wavenumber $k_1/k^*$ in the range (0.1, 5.0) for two selected angles $u_{12} = 30°$ and $u_{12} = 70°$. The zero crossings are indicated by thick contour lines.

Let us introduce the parameters representing two conserved quantities:

$$j_* = \frac{|J_1 - J_2|}{J_m} \geqslant 0, \qquad r = \alpha' J_m^{1/2}. \tag{5.13}$$

The parameter $j_*$ measures the difference between the maximum attainable wave actions of the two longer waves, see figure 3. The parameter $r$ is proportional to the maximum amplitude attainable by the shortest wave.

In figure 4 we show contour plots for the coefficient $\beta$ as a function of the wavenumber $k_1$ and the angle $v_1$ for $u_{12} = 30°$ and $u_{12} = 70°$. In general, when the angle $u_{12}$ between the resonating waves is small, $\beta$ is insensitive to variations in the angle of incidence of the long wave $v_1$. When the angle between the resonating waves is large, $\beta$ varies significantly with the long-wave angle of incidence. If $u_{12} > 44°$ (approximately), it is possible to have $\beta = 0$ while the interaction coefficients $\beta_1, \beta_2, \beta_3$ are individually non-zero. The zero crossings of $\beta$ are plotted as thick contour curves on the surface. When $\beta$ vanishes, the influence of the long wave is not dynamically significant for the triad *at this order*, and will only give a trivial phase shift.

In terms of $j$ and $\psi$ the dynamical system becomes

$$\frac{\mathrm{d}j}{\mathrm{d}t} = -r\,[(1-j)j(j+j_*)]^{1/2}\sin\psi \;=\; \frac{\partial H}{\partial \psi}, \tag{5.14a}$$

$$\frac{\mathrm{d}\psi}{\mathrm{d}t} = r\frac{3j^2 - 2j + 2j_* j - j_*}{2\,[(1-j)j(j+j_*)]^{1/2}}\cos\psi + \Delta + \beta\cos t \;=\; -\frac{\partial H}{\partial j}, \tag{5.14b}$$

where $H$ is the time-dependent Hamiltonian defined by

$$H(j,\psi;t) = r\,[(1-j)j(j+j_*)]^{1/2}\cos\psi - (\Delta+\beta\cos t)j. \tag{5.15}$$

In the special case of $j_* = 0$, the equations (5.14) can be substantially simplified. This occurs when the two longer waves (wavenumbers $\boldsymbol{k}_1$ and $\boldsymbol{k}_2$) have the same wave action. A special case is Wilton's ripples, for which the two longer waves are identical ($\boldsymbol{k}_1 = \boldsymbol{k}_2$).

We remark that laboratory experiments in the literature fall into two categories. They either consider collinear Wilton's ripples (e.g. McGoldrick 1970; Henderson & Hammack 1987) or they correspond to the initial condition that only the shortest wave has finite amplitude, while the two longer waves start out with infinitesimal amplitudes (e.g. Banerjee & Korpel 1982; Henderson & Hammack 1987; Perlin *et al.* 1990). Hence all of these experiments correspond to $j_* = 0$.

## 6. Analytical solution without the long wave

In the absence of the long wave ($\beta = 0$), the temporal solution of the conservative three-wave equations is well known (see Craik 1985). In order to facilitate the subsequent analysis of the effect of the long wave, we first summarize the known analytical solution, and illustrate properties of the phase portrait and the bifurcations that may occur due to detuning. In particular we point out that the bifurcation criterion found previously for certain special triad configurations (Chen & Saffman 1979; Reeder & Shinbrot 1981; Ma 1982) can be extended to an arbitrary resonating triad as long as the wave actions of the two longer waves are equal.

The variable $\psi$ can be eliminated from the system (5.14) by using the Hamiltonian (5.15). The resulting equation for $j$ is

$$\frac{\mathrm{d}j}{\mathrm{d}t} = \pm r\left[(1-j)j(j+j_*) - (H+\Delta j)^2\right]^{1/2} = \pm r\,[(h_2-j)(j-h_1)(j-h_0)]^{1/2}, \tag{6.1}$$

where $h_0$, $h_1$ and $h_2$ are the zeros of the radicand. We let $h_0 \leqslant 0 \leqslant h_1 \leqslant j \leqslant h_2 \leqslant 1$, such that $h_1$ and $h_2$ are the lower and upper bounds for $j$.

If we take the initial condition $j(0) = h_2$, the negative sign must be taken in (6.1), and the solution is

$$j(t) = h_2 - (h_2-h_1)\,\mathrm{sn}^2(\tfrac{1}{2}rt(h_2-h_0)^{1/2}, m), \qquad m = \left(\frac{h_2-h_1}{h_2-h_0}\right)^{1/2}. \tag{6.2}$$

Here sn is a Jacobi elliptic function, and the parameter $m$ is defined according to Gradshteyn & Ryzhik (1980). The period $\mathscr{T}$ of modulational oscillation is given by the complete elliptic integral of the first kind,

$$\mathscr{T} = \frac{4}{r(h_2-h_0)^{1/2}}\,\mathrm{K}(m). \tag{6.3}$$

These results are well known.

The parameter $m$ is in the range $0 \leqslant m \leqslant 1$. In the limit $m = 0$, we have $h_1 = h_2$ and the solution reduces to a fixed point (a centre) at $j = j_c$ and $\psi = \psi_c$. Here $\psi_c$ is either 0 or $\pi$ and $j_c$ is the solution of

$$(3j_c^2 - 2j_c + 2j_*j_c - j_*)\cos\psi_c = -\frac{2\Delta}{r}\,[(1-j_c)j_c(j_c+j_*)]^{1/2}. \tag{6.4}$$

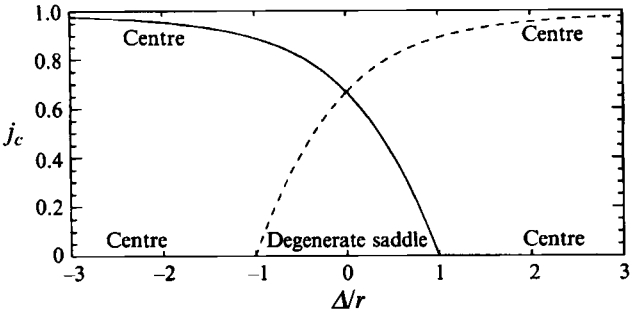


FIGURE 5. Bifurcation diagram for the location $j_c$ of centres when $j_* = 0$ and $-3 < \Delta/r < 3$. $j_c = 0$ is a fixed point for all $\Delta/r$. The generalized bifurcation of Chen & Saffman (1979) is seen at $j_c = 0$ and $\Delta/r = \pm 1$. Solid line $\psi_c = 0$, dashed line $\psi_c = \pi$.

Of particular interest is the special case when $j_* = 0$; the solution is then

$$j_c = \frac{6 - 2(\Delta/r)^2 \pm 2\left((\Delta/r)^4 + 3(\Delta/r)^2\right)^{1/2}}{9}, \tag{6.5}$$

see figure 5. By linearization of (5.14) about the fixed point $(j_c, \psi_c)$, we can verify that it is a centre with the frequency

$$\lambda = r\left(3j_c - 1 + j_* + (\Delta/r)^2\right)^{1/2}, \tag{6.6}$$

in accordance with (6.3) for $m = 0$.

For further insight into the behaviour in terms of the variables $j$ and $\psi$, it is convenient to regard these as coordinates on a sphere, with $j$ measuring the latitude, and $\psi$ the longitude. Thus $j = 0$ (only the shortest wave is present) corresponds to the south pole and $j = 1$ (the shortest wave is absent) the north pole. We perform local analyses at the poles to understand the behaviour there.

Near the south pole $j = 0$, i.e. when the shortest wave $\boldsymbol{k}_3$ is dominating over the other two waves in the triad, we introduce new coordinates

$$x = j^{1/2}\cos\psi, \qquad y = j^{1/2}\sin\psi \tag{6.7}$$

in (5.14). When $j_* > 0$, we get to the zeroth order in $x$ and $y$,

$$\frac{\mathrm{d}x}{\mathrm{d}t} = 0, \qquad \frac{\mathrm{d}y}{\mathrm{d}t} = -\frac{r j_*^{1/2}}{2}. \tag{6.8}$$

Hence the south pole has a finite flow in the negative $y$-direction. For $j_* = 0$, the above approximation is inadequate, and it is more convenient to return to the polar representation. To the zeroth order in $j^{1/2}$, we have

$$\frac{\mathrm{d}j^{1/2}}{\mathrm{d}t} = 0, \qquad \frac{\mathrm{d}\psi}{\mathrm{d}t} = -r\cos^3\psi + \Delta. \tag{6.9}$$

The south pole is now a fixed point. When $|\Delta/r| > 1$, it is a centre. When $|\Delta/r| < 1$, it resembles a saddle point, with invariant stable and unstable eigenspaces along the two lines ($\psi$ constant) determined by

$$\cos^3\psi = \Delta/r. \tag{6.10}$$

Because there is only one stable and one unstable eigendirection, we call this fixed point a degenerate saddle.

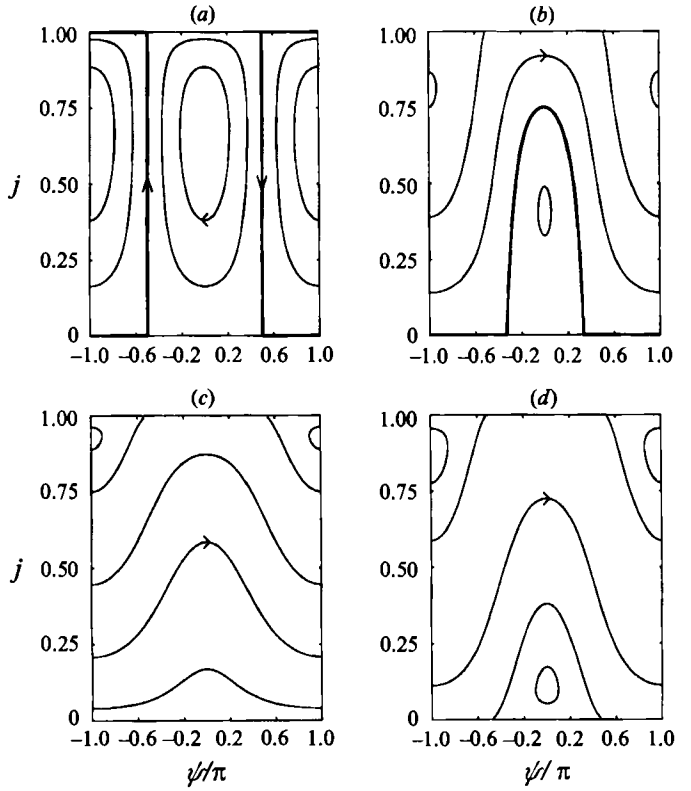


FIGURE 6. Phase portraits $(j,\psi)$ for the autonomous system. (*a*) $j_* = 0$, $\Delta/r = 0$; (*b*) $j_* = 0$, $\Delta/r = 0.5$; (*c*) $j_* = 0$, $\Delta/r = 1.5$; (*d*) $j_* = 1$, $\Delta/r = 1.5$. The homoclinic trajectory is drawn as a thick line in (*a*) and (*b*).

By a similar analysis it can be shown that the north pole $j = 1$ (i.e. the shortest wave is not present) is never a fixed point.

The stable and unstable eigendirections of the degenerate saddle are part of a homoclinic trajectory. This occurs in the limit $m = 1$, and the solution reduces to

$$j = (1 - (\Delta/r)^2)\,\mathrm{sech}^2\,\frac{rt}{2}. \tag{6.11}$$

This happens only when $j_* = 0$ and

$$|\Delta/r| < 1. \tag{6.12}$$

Chen & Saffman (1979) discussed the bifurcations of steady solutions for collinear Wilton's ripples. They gave the criterion that if the height ($h$) of a steady second-harmonic wave (wavenumber $2k$) exceeds

$$h > \frac{4}{3k}\left|\frac{Tk^2}{\rho g} - \frac{1}{2}\right|, \tag{6.13}$$

then the second-harmonic wave can bifurcate into a steady combination wave of the first and second harmonics. To the leading order in detuning, their condition is a special limit of the bifurcation condition (6.12), in the special case of Wilton's ripples. The bifurcation can be seen in figure 5 as the branching of the centre curve (6.5) away from $j_c = 0$. At the branch point, $j_c = 0$ changes from being a centre to a saddle.

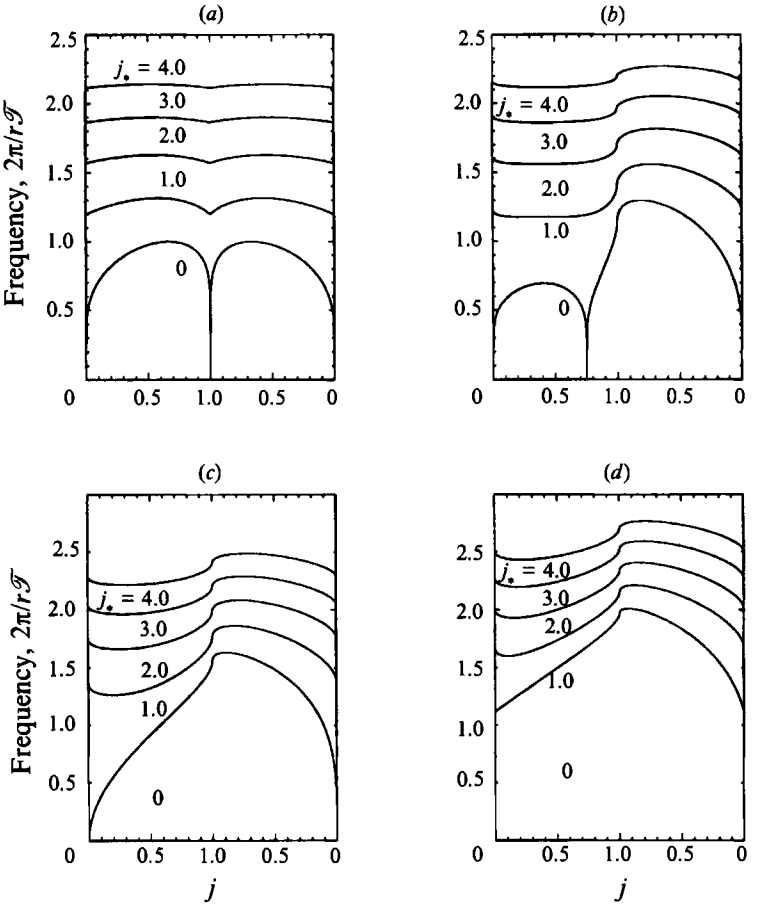


FIGURE 7. Frequency of envelope oscillation, $2\pi/r\mathscr{T}$, of the autonomous system. Along the horizontal axis, $j$ first increases from 0 to 1 corresponding to $\psi = 0$, then decreases from 1 to 0 corresponding to $\psi = \pi$. (*a*) $\Delta/r = 0$, (*b*) $\Delta/r = 0.5$, (*c*) $\Delta/r = 1$, (*d*) $\Delta/r = 1.5$

To see that (6.12) reduces to (6.13) for Wilton's ripples, we drop the ordering parameter $\epsilon$, and set

$$k_1 = k_2 = \tfrac{1}{2}k_3 = \left(\frac{g}{2\gamma}\right)^{1/2} \qquad \text{and} \qquad \delta_1 = \delta_2 = \tfrac{1}{2}\delta_3 = k - k_1.$$

Our condition (6.12) then becomes

$$h > \frac{4}{3k}\left|\frac{\gamma k^2}{g} - \frac{1}{2} - \frac{\delta_1}{2k_1}\right|,$$

which is the same as (6.13) within the order of the detuning $O(\delta_1/k_1) = O(\epsilon)$.

We have now shown that this bifurcation can occur for any resonating triad, as long as $j_* = 0$, i.e. whenever the wave actions of the two longer waves are equal. The existence of the degenerate saddle point, which is predicted by the bifurcation condition, is found to have an important consequence for the onset of chaotic behaviour in the presence of a long wave.

The possible phase portraits are simply contours of constant Hamiltonian, some of which are presented in figure 6. The two important parameters that determine the qualitative phase-space behaviour are $j_*$ and $|\Delta/r|$. When $j_* > 0$, there are only two centres, at $\psi = 0$ and $\psi = \pi$, and with $0 < j_c < 1$. When $j_* = 0$ there are two centres, and if $|\Delta/r| < 1$ there is an additional degenerate saddle point. The homoclinic trajectory is highlighted as a thick curve in figure 6.

In figure 7 the frequency of the closed orbits, $2\pi/r\mathscr{T}$, is plotted as a function of the value of $j$ where the orbits cross $\psi = 0$ or $\psi = \pi$, for selected values of $j_*$ and $\Delta/r$. The value along the abscissa ($j$) first increases from 0 to 1 corresponding to $\psi = 0$, and then decreases from 1 back to 0 corresponding to $\psi = \pi$. While the homoclinic orbit is non-periodic with zero frequency, large values of $j_*$ causes all orbits to have approximately the same frequency. This has an important consequence in our later analysis of the effect of the long wave: When there is a broad range of natural oscillation frequencies, the triad can be resonantly exited more easily by the long wave. The broadest range of natural frequencies happens for $j_* = 0$ and moderate detuning.

## 7. Effects of a weak long wave near the centre

We now come to the main objective of this paper, which is the effect of the long wave on the triad. In this section we derive approximate analytical results by assuming that the long-wave forcing coefficient $\beta$ is sufficiently small that a perturbation approach can be employed. Numerical confirmation by integration of the original evolution equations is presented afterwards. In the next section we consider stronger long-wave disturbance numerically.

Corresponding to the closed orbits, the typical behaviour of triad resonance is the periodic modulation of the envelopes, found analytically in §6. If the period of the long wave is on the same timescale, the natural modulational oscillations of the envelope may then be resonated. We denote this *modulational resonance*, to distinguish it from the basic wave resonance between the three short waves.

A convenient way to present the behaviour of the disturbed triad, is to use the Poincaré map (or first return map), for which the state of the triad is periodically sampled with a time interval equal to the period of the long-wave oscillation. Since the long-wave frequency has been normalized to unity, this corresponds to sampling at times $t = 2\pi n$ for $n = 1, 2, 3, \ldots$.

We first carry out a perturbation analysis for the case of no modulational resonance, and then consider two cases of modulational resonances. Specifically, a small parameter $\mu \ll 1$ will be used to characterize the envelope modulation, and will be distinguished from $\epsilon \ll 1$ in the original perturbation analysis. We use the normalized time coordinate $t$ as defined by (5.5), to be the basic time for modulation of the envelope. Within the basic time range of $t = O(1)$, we allow a cascade of slow times $\mu t, \mu^2 t, \ldots$. In this section, indices always refer to the order in terms of $\mu$.

The starting equations are (5.14). It suffices to consider only perturbations around the centre at $\psi_c = 0$. By the symmetry of the governing equations, the solution near $\psi_c = \pi$ can be obtained by translating $\psi \to \pi - \psi$ and changing the signs of $\beta$ and $\Delta$. For simplicity, we consider only $\Delta = 0$, with extensions for $\Delta \neq 0$ being straightforward.

### 7.1. *Non-resonant long wave*

Let us assume that the long wave is weak such that $\beta = \mu\beta_1$. We also assume a slow modulational time $\tau = \mu^2 t$. Solutions will be sought in the perturbation expansions

$$j = j_c + \mu j_1 + \mu^2 j_2 + \mu^3 j_3 + \cdots, \tag{7.1a}$$

$$\psi = \psi_c + \mu\psi_1 + \mu^2\psi_2 + \mu^3\psi_3 + \cdots, \tag{7.1b}$$

where all $j_n$, $\psi_n$ depend on the fast and the slow times.

We choose to express $j_*$ in terms of $j_c$, according to (6.4), i.e.

$$j_* = \frac{2j_c - 3j_c^2}{2j_c - 1}. \tag{7.2}$$

In order to simplify the equations, we introduce the notation

$$\mathscr{R} \equiv (2j_c - 1)^{1/2}, \qquad \mathscr{S} \equiv (3j_c^2 - 3j_c + 1)^{1/2}. \tag{7.3}$$

At the leading order $O(\mu)$, we get

$$\frac{\mathrm{d}j_1}{\mathrm{d}t} - \frac{(j_c - 1)j_c r}{\mathscr{R}}\psi_1 = 0, \tag{7.4a}$$

$$\frac{\mathrm{d}\psi_1}{\mathrm{d}t} + \frac{\mathscr{S}^2 r}{(j_c - 1)j_c\mathscr{R}}j_1 = \beta_1 \cos t. \tag{7.4b}$$

These are the equations for a linear oscillator with a natural frequency $\lambda$ given by (6.6), but forced at the frequency 1. The first-order response must therefore be of the form

$$j_1 = p_1 \mathrm{e}^{\mathrm{i}\lambda t} + q_1 \mathrm{e}^{\mathrm{i}t} + \text{c.c.}, \tag{7.5a}$$

$$\psi_1 = r_1 \mathrm{e}^{\mathrm{i}\lambda t} + s_1 \mathrm{e}^{\mathrm{i}t} + \text{c.c.} \tag{7.5b}$$

The complex amplitudes of the free oscillation, $p_1$ and $r_1$, are so far arbitrary, while the amplitudes of the forced oscillation, $q_1$ and $s_1$, are constants. Their detailed forms are not of particular interest, and are omitted here.

Owing to nonlinear interactions and the long wave, the following harmonics will be forced at the first three orders of $\mu$:

$$\left.\begin{array}{ll} O(\mu) & 1 \\ O(\mu^2) & 2\lambda,\ \lambda+1,\ \lambda-1,\ 2,\ 0 \\ O(\mu^3) & 3\lambda,\ 2\lambda+1,\ 2\lambda-1,\ \lambda+2,\ \lambda-2,\ \lambda,\ 3,\ 1. \end{array}\right\} \tag{7.6}$$

In this subsection we assume that all of the other harmonics listed above are different from $\lambda$. We must then allow $p_1$ to vary with $\tau$ in order to avoid secular forcing of frequency $\lambda$ at $O(\mu^3)$.

At the second order in $\mu$, we have

$$\frac{\mathrm{d}j_2}{\mathrm{d}t} - \frac{(j_c - 1)j_c r}{\mathscr{R}}\psi_2 = 0, \tag{7.7a}$$

$$\frac{\mathrm{d}\psi_2}{\mathrm{d}t} + \frac{\mathscr{S}^2 r}{(j_c - 1)j_c\mathscr{R}}j_2 = -\frac{3r\mathscr{R}}{2(j_c - 1)j_c}j_1^2. \tag{7.7b}$$

The solution is of the form

$$j_2 = p_{20} + p_{21}\mathrm{e}^{\mathrm{i}\lambda t} + p_{22}\mathrm{e}^{2\mathrm{i}\lambda t} + p_{23}\mathrm{e}^{\mathrm{i}(\lambda+1)t} + p_{24}\mathrm{e}^{\mathrm{i}(\lambda-1)t} + q_{22}\mathrm{e}^{2\mathrm{i}t} + \text{c.c.}, \tag{7.8a}$$

$$\psi_2 = r_{20} + r_{21}\mathrm{e}^{\mathrm{i}\lambda t} + r_{22}\mathrm{e}^{2\mathrm{i}\lambda t} + r_{23}\mathrm{e}^{\mathrm{i}(\lambda+1)t} + r_{24}\mathrm{e}^{\mathrm{i}(\lambda-1)t} + s_{22}\mathrm{e}^{2\mathrm{i}t} + \text{c.c.} \tag{7.8b}$$

The solutions of the coefficients are omitted here for brevity.

At the third order, we have

$$\frac{\mathrm{d}j_3}{\mathrm{d}t} - \frac{(j_c-1)j_c r}{\mathscr{R}}\psi_3 = -\frac{\mathscr{S}^2 r}{2(j_c-1)j_c\mathscr{R}} j_1^2\psi_1 - \frac{(j_c-1)j_c r}{6\mathscr{R}}\psi_1^3 - \frac{\mathrm{d}j_1}{\mathrm{d}\tau}, \tag{7.9a}$$

$$\frac{\mathrm{d}\psi_3}{\mathrm{d}t} + \frac{\mathscr{S}^2 r}{(j_c-1)j_c\mathscr{R}} j_3 = \frac{\mathscr{S}^2 r}{2(j_c-1)j_c\mathscr{R}} j_1\psi_1^2 - \frac{\mathscr{S}^2 r}{2(j_c-1)^3 j_c^3\mathscr{R}} j_1^3 - \frac{3r\mathscr{R}}{(j_c-1)j_c} j_1 j_2 - \frac{\mathrm{d}\psi_1}{\mathrm{d}\tau}. \tag{7.9b}$$

The natural oscillation frequency is now forced through the nonlinear terms on the right-hand-side. Solvability for $p_{31}$ leads to the following condition for $p_1$:

$$\frac{\mathrm{d}p_1}{\mathrm{d}\tau} + \mathrm{i}C_1 p_1 |p_1|^2 + \mathrm{i}C_2 p_1 = 0, \tag{7.10}$$

where $C_1$ and $C_2$ are functions of $j_c$ and $\lambda$.

The evolution equation (7.10) is readily solved, subject to the initial condition $p_1(0) = P$,

$$p_1 = P\mathrm{e}^{-\mathrm{i}(C_1|P|^2 + C_2)\tau}. \tag{7.11}$$

The expansion for $j$ becomes

$$j = j_c + 2\mu\mathrm{Re}\left\{p_1(\mu^2 t)\mathrm{e}^{\mathrm{i}\lambda t} + q_1\mathrm{e}^{\mathrm{i}t}\right\} + O(\mu^2), \tag{7.12}$$

with a similar expansion for $\psi$. Physically, the slow modulation due to (7.10) gives a small correction to the natural oscillation frequency. The resulting modulation of the wave amplitude is simply a superposition of discrete simple harmonic oscillations.

The perturbation results have been confirmed with numerical integrations of the full evolution equations. As an example, let us fix $r = 0.7$, $j_* = 2.$, $\beta = 0.1$, $\Delta = 0$, and take the initial condition $(j, \psi) = (0.6, 0)$. Figure 8 shows the phase-plane trajectory for a duration of 50. Superimposed as a thick curve is the Poincaré (first return) map, as described above. Figure 9 shows $10\log_{10}$ of the magnitude of the Fourier transform of $j(t)$. An FFT of size 8192 was used with a time step of 0.105. The frequencies and amplitudes of the first and second harmonics, as predicted by this perturbation theory, are indicated by asterisks. The asterisks are plotted with the corrected frequency, which takes into account the slow modulation predicted by (7.10). The approximate analysis gives an accurate prediction of the dominant frequencies and their amplitudes. The approximate analysis works quite well even when the amplitude $|j - j_c|$ is not small.

From the list in (7.6) it can be seen that modulational resonance may occur at first order in $\mu$ if $\lambda = 1$, at second order if $\lambda$ is $\frac{1}{2}$ or 2, and at third order if $\lambda$ is $\frac{1}{3}$ or 3. In principle there may be modulational resonance for $\lambda$ equal to any rational number for some order of $\mu$. In the next two subsections, we consider in some detail the cases $\lambda = 1$ and $\lambda = \frac{1}{2}$. All the other resonant cases up to the third order have been worked out, after lengthy but straightforward analysis. They are not repeated here.

### 7.2. *First-order synchronous modulational resonance, $\lambda = 1$*

For synchronous modulational resonance we set

$$\lambda = 1 + f, \tag{7.13}$$

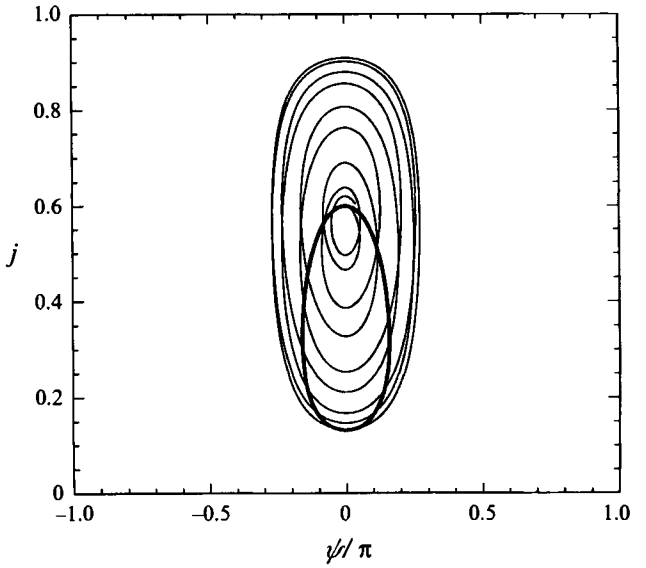


FIGURE 8. Numerically computed trajectory $(j, \psi)$ (thin line) for $\beta = 0.1$, $r = 0.7$, $j_* = 2$ and $\Delta = 0$. The system evolved from the initial condition $(j, \psi) = (0.6, 0)$ until time $t = 50$. The Poincaré map, sampling every long-wave period $t = 2\pi n$, is indicated by the thick curve.

where $f$ denotes detuning of the natural frequency from the forcing frequency. We choose to express $r$ in terms of $f$ and $j_c$, see (6.6) and (7.3):

$$r = (1 + f)\frac{\mathscr{R}}{\mathscr{S}}. \tag{7.14}$$

In order to balance slow growth and nonlinearity, let us assume a weak long wave, small detuning and slow time according to the following scales:

$$\beta = \mu^3 \beta_3, \qquad f = \mu^2 f_2, \qquad \tau = \mu^2 t. \tag{7.15}$$

Perturbation expansions of the form (7.1) with $\psi_c = 0$ are assumed, where all $j_n$ and $\psi_n$ depend on the fast and the slow time.

At leading order, we get

$$\frac{\mathrm{d}j_1}{\mathrm{d}t} - \frac{(j_c - 1)j_c}{\mathscr{S}}\psi_1 = 0, \quad \frac{\mathrm{d}\psi_1}{\mathrm{d}t} + \frac{\mathscr{S}}{(j_c - 1)j_c} j_1 = 0. \tag{7.16a,b}$$

This is an oscillator with natural frequency 1. We therefore assume the response

$$j_1 = p_1 \mathrm{e}^{\mathrm{i}t} + \text{c.c.}, \qquad \psi_1 = \frac{\mathrm{i}\mathscr{S}}{(j_c - 1)j_c} p_1 \mathrm{e}^{\mathrm{i}t} + \text{c.c.} \tag{7.17}$$

The complex amplitudes are functions of the slow time $\tau$.

At the second order, we have

$$\frac{\mathrm{d}j_2}{\mathrm{d}t} - \frac{(j_c - 1)j_c}{\mathscr{S}}\psi_2 = 0, \tag{7.18a}$$

$$\frac{\mathrm{d}\psi_2}{\mathrm{d}t} + \frac{\mathscr{S}}{(j_c - 1)j_c} j_2 = -\frac{3(2j_c - 1)}{2(j_c - 1)j_c \mathscr{S}} j_1^2. \tag{7.18b}$$

The second-order system is not forced at the natural frequency. We assume the

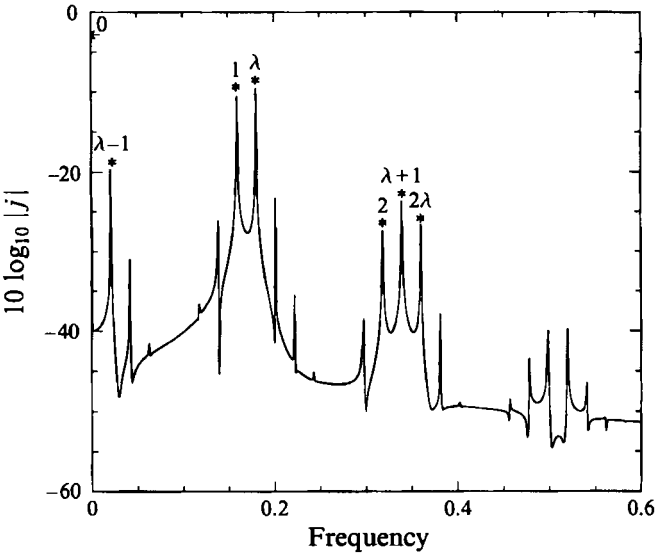


FIGURE 9. Fourier spectrum of $j(t)$ for the trajectory shown in the previous figure. The continuous curve is the FFT computed with 8192 samples and time step 0.105. The asterisks are the analytically computed Fourier amplitudes according to our perturbation analysis, with the frequencies adjusted to compensate for slow time modulation. The natural modulation frequency is $\lambda$ and the forcing frequency due to the long wave is unity (1). The expressions for the amplitudes are omitted in the text.

solution

$$j_2 = p_{20} + p_{21}\mathrm{e}^{\mathrm{i}t} + p_{22}\mathrm{e}^{2\mathrm{i}t} + \text{c.c.}, \tag{7.19a}$$

$$\psi_2 = r_{20} + r_{21}\mathrm{e}^{\mathrm{i}t} + r_{22}\mathrm{e}^{2\mathrm{i}t} + \text{c.c.} \tag{7.19b}$$

Again, the complex amplitudes are functions of $\tau$.

At the third order, we have

$$\frac{\mathrm{d}j_3}{\mathrm{d}t} - \frac{(j_c-1)j_c}{\mathscr{S}}\psi_3 = -\frac{(j_c-1)j_c}{6\mathscr{S}}\psi_1^3 + \frac{(j_c-1)j_c}{\mathscr{S}}f_2\psi_1 - \frac{\mathscr{S}}{2(j_c-1)j_c}j_1^2\psi_1 - \frac{\mathrm{d}j_1}{\mathrm{d}\tau}, \tag{7.20a}$$

$$\frac{\mathrm{d}\psi_3}{\mathrm{d}t} + \frac{\mathscr{S}}{(j_c-1)j_c}j_3 = \frac{\mathscr{S}}{2(j_c-1)j_c}j_1\psi_1^2 - \frac{\mathscr{S}}{(j_c-1)j_c}f_2 j_1 + \beta_3\cos t - \frac{\mathrm{d}\psi_1}{\mathrm{d}\tau} - \frac{3(2j_c-1)}{(j_c-1)j_c\mathscr{S}}j_1 j_2 - \frac{1}{2}\left[\frac{\mathscr{S}}{(j_c-1)j_c}\right]^3 j_1^3. \tag{7.20b}$$

This problem is forced at its natural frequency. Hence we impose a solvability condition, to avoid secular growth of the first-harmonic response. This leads to the following slow evolution equation for the complex amplitude $p_1$:

$$\frac{\mathrm{d}p_1}{\mathrm{d}\tau} + \mathrm{i}A_1|p_1|^2 p_1 - \mathrm{i}f_2 p_1 - \mathrm{i}A_2\beta_3 = 0, \tag{7.21}$$

where the real and non-negative coefficients $A_1$ and $A_2$ are

$$A_1 = \frac{15(2j_c-1)^2}{4\mathscr{S}^4}, \qquad A_2 = \frac{(1-j_c)j_c}{4\mathscr{S}}. \tag{7.22}$$

The complex evolution equation can be written as two coupled real equations, by

introducing $p_1 = x + iy$:

$$\frac{d}{d\tau}\begin{pmatrix} x \\ y \end{pmatrix} = \begin{pmatrix} A_1 y(x^2+y^2) - f_2 y \\ -A_1 x(x^2+y^2) + f_2 x + A_2\beta_3 \end{pmatrix} = \begin{pmatrix} \partial h/\partial y \\ -\partial h/\partial x \end{pmatrix} \tag{7.23}$$

where $h$ is the Hamiltonian

$$h(x,y) = \tfrac{1}{4}A_1(x^2+y^2)^2 - \tfrac{1}{2}f_2(x^2+y^2) - A_2\beta_3 x. \tag{7.24}$$

Hence the trajectories of $(x,y)$ are easily plotted as the level curves of $h$.

From the leading-order solution (7.17), it is seen that the Poincaré map of the original $(j,\psi)$-system is

$$j(2\pi n) = j_c + 2\mu x_n + O(\mu^2), \tag{7.25}$$

$$\psi(2\pi n) = \psi_c - \frac{2\mu\mathscr{S}}{(j_c-1)j_c} y_n + O(\mu^2), \tag{7.26}$$

where

$$\begin{pmatrix} x_n \\ y_n \end{pmatrix} = \begin{pmatrix} x \\ y \end{pmatrix}_{t=2\pi n\mu^2}. \tag{7.27}$$

Hence the invariant manifolds of the Poincaré map of $(j,\psi)$ are qualitatively similar to and approximated by the level curves of $h(x,y)$ after an appropriate linear transformation.

The bifurcation set of the system (7.23), written compactly as

$$\dot{x} = F(x,y,j_c,f,\beta), \quad \dot{y} = G(x,y,j_c,f,\beta), \tag{7.28}$$

is the set of parameter values $(j_c,f,\beta)$ where the system changes its qualitative behaviour. The bifurcation set is given as the solution of the three equations

$$F = 0, \qquad G = 0, \qquad \frac{\partial(F,G)}{\partial(x,y)} = 0. \tag{7.29}$$

The solution is readily found to be the union of the two surfaces

$$\left.\begin{array}{ll} S_1: & f_2 = \left(\frac{27}{4}A_2^2 A_1 \beta_3^2\right)^{1/3}, \\ S_2: & \beta_3 = 0, \quad f_2 \geqslant 0. \end{array}\right\} \tag{7.30}$$

The two surfaces divide the parametric space into three regions, as shown in figure 10. In each region we show typical phase portraits for $(x,y)$, which are qualitatively similar to the Poincaré map of $(j,\psi)$. In region I the map has one centre. In regions II and III the map has two centres and one saddle point. Two homoclinic manifolds connect back to the saddle point. The phase portraits in regions II and III are mirror reflections of each other, corresponding to the symmetries of the Hamiltonian $h(x,y)$.

### 7.3. *Second-order subharmonic modulational resonance, $\lambda = \frac{1}{2}$*

We set

$$\lambda = \tfrac{1}{2} + f, \tag{7.31}$$

and assume the following scales:

$$\beta = \mu^2\beta_2, \qquad f = \mu^2 f_2, \qquad \tau = \mu^2 t. \tag{7.32}$$

The leading-order natural response is assumed to be

$$j_1 = p_{1,1/2}e^{it/2} + \text{c.c.}, \qquad \psi_1 = \frac{i\mathscr{S}}{(j_c-1)j_c} p_{1,1/2}e^{it/2} + \text{c.c.} \tag{7.33}$$

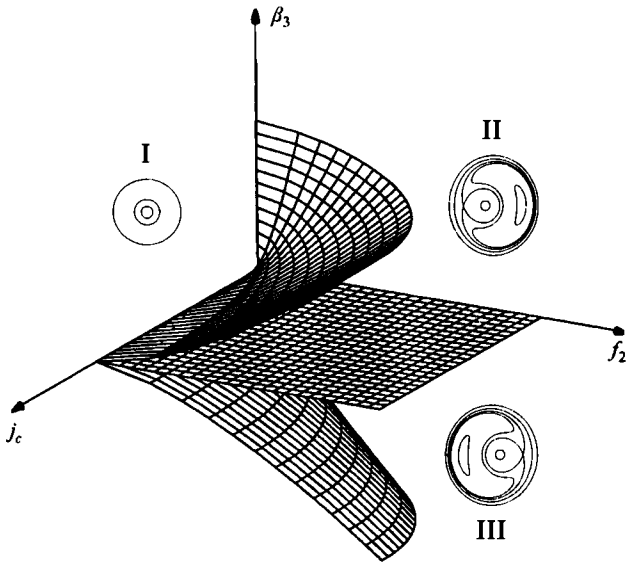


FIGURE 10. Bifurcation diagram for synchronous modulational resonance. The bifurcation surfaces are shown in the parameter space of $j_c$, $f_2$ and $\beta_3$. Typical phase portraits are shown in each region. In all portraits the horizontal and vertical axes are $x$ and $y$, respectively. Note the relative rotation of portraits in regions II and III.

Removal of secular growth at $O(\mu^3)$ now gives

$$\frac{\mathrm{d}p_{1,1/2}}{\mathrm{d}\tau} + \mathrm{i}A_1|p_{1,1/2}|^2 p_{1,1/2} - \mathrm{i}f_2 p_{1,1/2} - \mathrm{i}A_2\beta_2 p^*_{1,1/2} = 0, \tag{7.34}$$

where the real and non-negative coefficients $A_1$ and $A_2$ are

$$A_1 = \frac{15(2j_c - 1)^2}{8\mathscr{S}^4}, \qquad A_2 = \frac{(1 - j_c)j_c(2j_c - 1)}{4\mathscr{S}^3}. \tag{7.35}$$

The complex evolution equation can be written as two coupled real equations similar to (7.23) by introducing $p_{1,1/2} = x + \mathrm{i}y$. The Hamiltonian is now

$$h(x, y) = \tfrac{1}{4}A_1(x^2 + y^2)^2 - \tfrac{1}{2}f_2(x^2 + y^2) - \tfrac{1}{2}A_2\beta_2(y^2 - x^2). \tag{7.36}$$

The evolution equation (7.34) and the associated Hamiltonian (7.36) are now qualitatively different from (7.21) and (7.24), respectively.

It is now natural to redefine the Poincaré map, by choosing the sampling time equal to twice the period of the long wave, $t = 4\pi n$ for $n = 1, 2, 3, \ldots$. The Poincaré (second return) map is now given by

$$j(4\pi n) = j_c + 2\mu x_{2n} + O(\mu^2), \tag{7.37a}$$

$$\psi(4\pi n) = \psi_c - \frac{2\mu\mathscr{S}}{(j_c - 1)j_c} y_{2n} + O(\mu^2), \tag{7.37b}$$

where

$$\begin{pmatrix} x_{2n} \\ y_{2n} \end{pmatrix} = \begin{pmatrix} x \\ y \end{pmatrix}_{t=4\pi n\mu^2}. \tag{7.38}$$

The manifolds of the Poincaré (second return) map for $(j, \psi)$ are thus approximated by the level curves of $h(x, y)$ after an appropriate linear transformation.

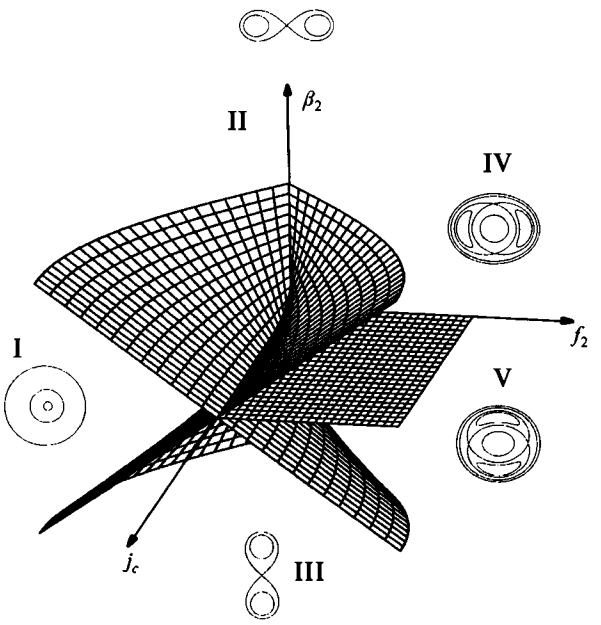


FIGURE 11. Bifurcation diagram for subharmonic $\frac{1}{2}$ modulational resonance. The bifurcation surfaces are shown in the parameter space of $j_c$, $f_2$ and $\beta_2$. Typical phase portraits are shown in each region. In all portraits the horizontal and vertical axes are $x$ and $y$, respectively. Note the relative rotation of portraits in regions II and III and in regions IV and V.

The bifurcation set is the union of the three surfaces

$$\left.\begin{array}{ll} S_1: & f_2 = -A_2|\beta_2|, \\ S_2: & f_2 = A_2|\beta_2|, \\ S_3: & \beta_2 = 0, \quad f_2 \geqslant 0. \end{array}\right\} \tag{7.39}$$

These three surfaces divide the parametric space into five regions, see figure 11. In each region we show typical phase portraits for $(x, y)$, which are identical to the level curves of $h(x, y)$, and which are qualitatively similar to the Poincaré (second return) map for $(j, \psi)$. We notice that the bifurcation surfaces are symmetric with respect to changing the sign of $\beta_2$, while the phase portraits for positive and negative $\beta_2$ can be obtained from each other by a 90° rotation. In region I the map has one centre. In regions II and III the map has two centres and one saddle point, with two homoclinic manifolds. In regions IV and V the map has three centres, two saddle points and four heteroclinic manifolds.

### 7.4. *Other resonances*

A similar analysis of the superharmonic resonances $\lambda = 2$ and $\lambda = 3$ reveals that they give a behaviour of the Poincaré map rather similar to the synchronous case $\lambda = 1$. The subharmonic resonance $\lambda = \frac{1}{3}$ is qualitatively different, in which case the parameter space is divided up into five regions, and one can have characteristic phase portraits involving three saddle points and four centres.

We have so far only considered the case of zero detuning $\Delta = 0$. When detuning and weak forcing are both present, the resulting modulational resonances and bifurcations can be anticipated with the help of figures 6 and 7. In particular, figure 12 shows a numerically computed Poincaré map for $\beta = 0.1$, $r = 0.7$, $j_* = 0$ and $\Delta = 0.7$.

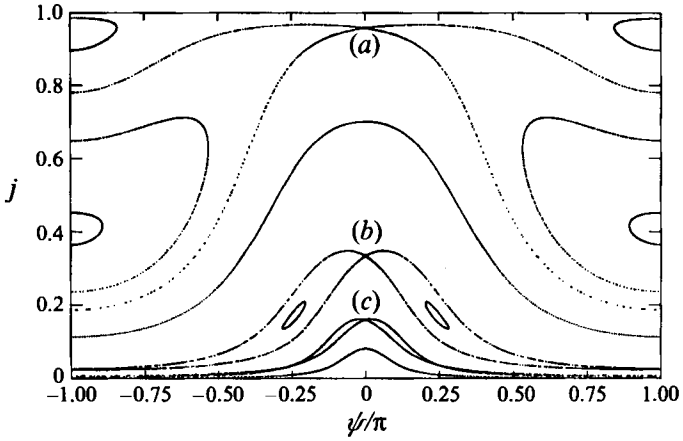


FIGURE 12. Poincaré map for $\beta = 0.1$, $r = 0.7$, $j_* = 0$ and $\Delta = 0.7$, showing the characteristic manifolds of synchronous resonance (*a*), subharmonic $\frac{1}{2}$ resonance (*b*) and subharmonic $\frac{1}{3}$ resonance (*c*).

The corresponding frequencies of closed orbits of the unforced system are shown in figure 7(*c*). The unforced system has no saddle points or homoclinic loops. It has two centres: the first at $j = 0$ with frequency 0 and the second at $(j = \frac{8}{9}, \psi = \pi)$ with frequency $\lambda = 1.4(\frac{2}{3})^{1/2} = 1.143$, according to (6.5) and (6.6). Since the unforced modulational oscillation frequency decreases monotonically from $\lambda = 1.143$ to 0 from the centre at $j = \frac{8}{9}$ to $j = 0$, we expect the occurrence of modulational resonances with frequencies 1, $\frac{1}{2}$, $\frac{1}{3}$ etc. at some intermediate locations when the forcing is weak. In figure 12 this can indeed be observed. The first centre of the unforced system can be traced at $j = 0$, while the second one is at $\psi = \pi$ and $j = 0.948$. Between these two centres (from north to south), we can see the resonant manifolds for synchronous resonance (*a*), subharmonic $\frac{1}{2}$ resonance (*b*) and subharmonic $\frac{1}{3}$ resonance (*c*).

In principle, there may be modulational resonance whenever the ratio between the oscillation frequency of natural modulations and the forcing frequency of the long wave is a rational number. A few resonances obtained by numerical integration are shown in figure 13, for parameter values $\beta = 0.1$, $r = 0.26$, $j_* = 0$ and $\Delta = 0$. The unforced system now has a degenerate saddle point at $j = 0$ with a homoclinic trajectory at $\psi = \pm\pi/2$. There are two centres at $j = \frac{2}{3}$, $\psi = 0$ and $\psi = \pi$, with frequency $\lambda = 0.26$, according to (6.4) and (6.6). Since the unforced modulational oscillation frequency decreases monotonically from $\lambda = 0.26$ at the two centres to 0 at the homoclinic trajectory, we expect the occurrence of various modulational resonances at some intermediate locations when the forcing is weak. In figure 13, we show the characteristic manifolds of four modulational resonances. Starting closest to the centres and going outward, we see a subharmonic $\frac{1}{4}$ resonance (*a*) inside a subharmonic $\frac{1}{5}$ resonance (*b*) inside a subharmonic $\frac{1}{6}$ resonance (*c*) inside a subharmonic $\frac{1}{7}$ resonance (*d*). These resonances are identified numerically as follows. We first locate any centre or saddle point of that resonance. Then we count how many iterations of the map are needed to get back to the same point. In doing so, we trace all the other centres or saddle points of the given resonant manifold as well. The plots showing the invariant manifolds of the saddle points have been generated by first finding the linear eigenspaces of each saddle point, and then taking a few initial

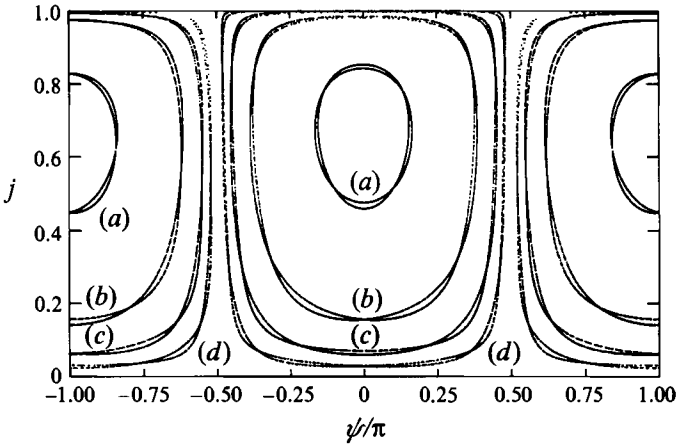


FIGURE 13. Poincaré map for $\beta = 0.1$, $r = 0.26$, $j_* = 0$ and $\Delta = 0$, showing the characteristic manifolds of subharmonic $\frac{1}{4}$ resonance ($a$), subharmonic $\frac{1}{5}$ resonance ($b$), subharmonic $\frac{1}{6}$ resonance ($c$) and subharmonic $\frac{1}{7}$ resonance ($d$).

conditions along these eigenspaces and iterating a few times forward and backward in time.

## 8. Effects of a stronger long-wave disturbance

Guided by the insight gained by the approximate analysis for weak long-wave disturbances, we have performed extensive numerical integration of the evolution equations. Because the reduced representation with $j$ and $\psi$ is singular at the poles of the sphere, we integrate the full six-dimensional system (5.7), and then transform the results to $j$ and $\psi$ for plotting. Presented below are the Poincaré maps obtained by sampling the state of the triad every long-wave period $t = 2\pi n$ for $n = 1, 2, 3, \ldots$.

We found in §6 that whenever $j_* = 0$ and $|\Delta/r| < 1$, the unforced system has a homoclinic trajectory connecting the degenerate saddlepoint at $j = 0$ to itself. We can show by a Melnikov analysis that the homoclinic trajectory will tangle and give rise to a stochastic behaviour for any small disturbance by the long wave. This is to be expected since our model does not include non-conservative effects. Thus whenever the conditions $j_* = 0$ and $|\Delta/r| < 1$ are satisfied, which is our generalization of the bifurcation condition of Chen & Saffman (1979), there are initial conditions that give rise to chaotic behaviour for an arbitrarily small long-wave disturbance.

In §7 we found homoclinic and heteroclinic manifolds of the Poincaré map, associated with modulational resonance. According to the analysis of §7, these manifolds should not tangle for a sufficiently weak long-wave disturbance. However, numerical computations show that these manifolds do tangle provided the long-wave disturbance is sufficiently large. Chaotic behaviour due to modulational resonance tends therefore to occur at a higher threshold value of the long-wave disturbance.

The Poincaré maps in figures 14 and 15 illustrate the behaviour of the triad subject to successively stronger disturbances by the long wave. We fix $j_* = 0$, $r = 0.55$, $\Delta = 0$ and let $\beta$ take the values 0.01, 0.1, 0.2, 1.2 and 2.0.

The weakest long-wave disturbance, $\beta = 0.01$ (figure 14) is within the validity of the perturbation theory, although the detuning from modulational resonance is rather large. We can see the characteristic heteroclinic manifolds of a subharmonic

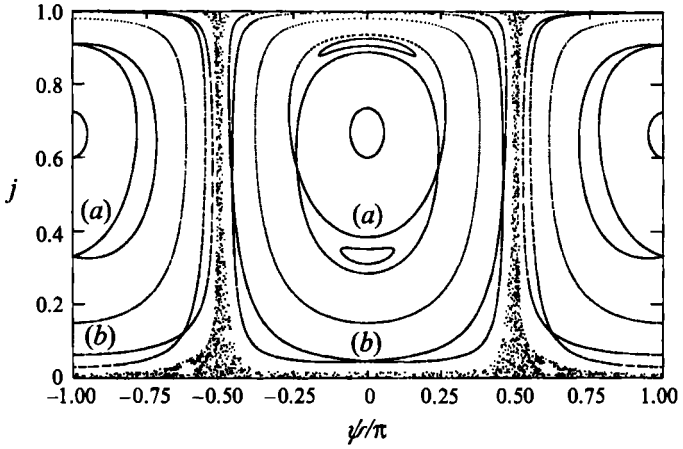


FIGURE 14. Poincaré map for $r = 0.55$, $j_* = 0$, $\Delta = 0$, $\beta = 0.01$. We see subharmonic $\frac{1}{2}$ modulational resonance ($a$) and subharmonic $\frac{1}{3}$ modulational resonance ($b$).

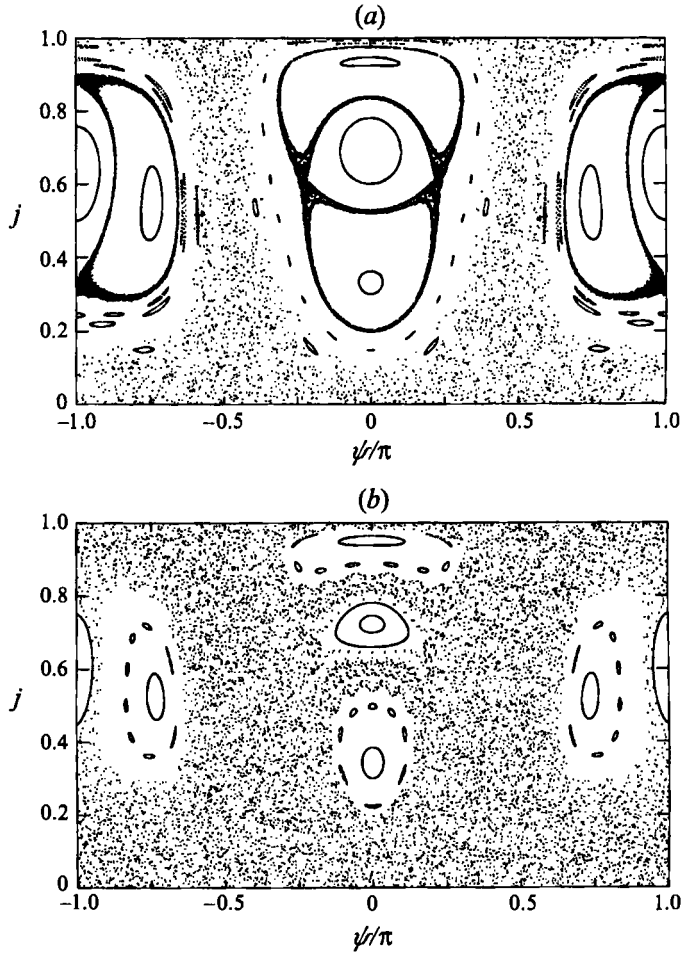


FIGURE 15. Poincaré map for $r = 0.55$, $j_* = 0$, $\Delta = 0$: ($a$) $\beta = 0.1$, ($b$) $\beta = 0.2$.

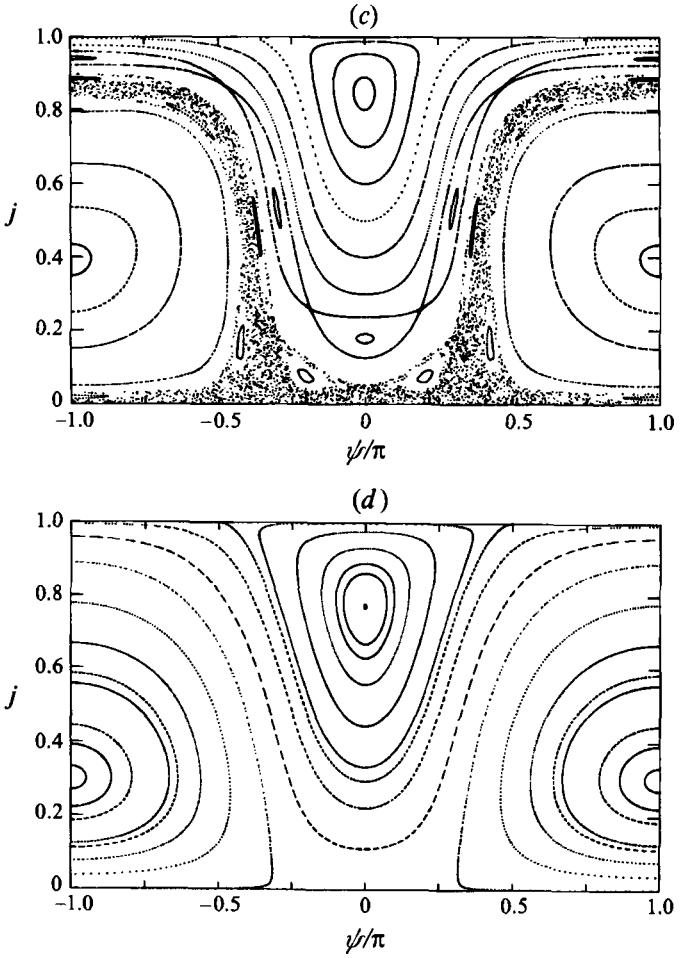


FIGURE 15. Poincaré map for $r = 0.55$, $j_* = 0$, $\Delta = 0$: (c) $\beta = 1.2$, (d) $\beta = 2.0$.

$\frac{1}{2}$ modulational resonance (*a*), corresponding to regions IV and V in figure 11. On the outside, we see the manifolds of a subharmonic $\frac{1}{3}$ modulational resonance (*b*), for which a perturbation theory has been worked out in the style of §7, but is not presented here for brevity. The disturbance by the long wave is sufficiently small that these heteroclinic manifolds do not tangle. The homoclinic trajectory of the autonomous system (see the thick curve in figure 6*a*) does tangle and gives rise to a stochastic layer, in accordance with the Melnikov analysis.

When $\beta = 0.1$ (figure 15*a*), the stochastic layer of the homoclinic trajectory of the autonomous system has grown in size to cover the area occupied by the subharmonic $\frac{1}{3}$ resonant manifold. The subharmonic $\frac{1}{2}$ resonant heteroclinic manifolds are now tangling and forming their own stochastic layers, which are separate from the stochastic layer of the homoclinic trajectory.

When $\beta = 0.2$ (figure 15*b*), the subharmonic $\frac{1}{2}$ tangle has joined with the tangle of the homoclinic trajectory of the autonomous system. Only small islands of phase space remain that are not covered by stochastic layers.

In general, as the long-wave disturbance increases, the stochastic layers will grow in size, and will eventually cover the entire phase space. Numerical experience indicates

however that when the long-wave disturbance becomes much larger, the chaotic behaviour may recede by the shrinking and disappearance of the stochastic layers. This is illustrated in figure 15(*c*) for $\beta = 1.2$. Here we can see that the area of phase space covered with stochastic layers has diminished.

In figure 15(*d*), $\beta = 2.0$ is sufficiently large that the dynamical behaviour is non-chaotic throughout phase space.

It is now clear that chaotic behaviour tends to develop first near the homoclinic trajectory of the autonomous system. The existence of such a trajectory is of course predicted by the bifurcation condition (6.12). For an increasingly strong long wave, chaos may then develop near the manifolds of modulational resonances. The greatest likelihood for modulational resonance to occur is when there is a wide range of natural modulational frequencies available. From figure 7, which shows the natural modulational frequencies, it is clear that a wide range is available when $j_*$ is small and $\Delta/r$ is of unit magnitude or smaller. In physical terms, this means that the wave actions of the two longer waves should be approximately equal, and the mismatch in the resonance condition should be small. Then chaotic behaviour of a triad is easily excited by a passing long wave.

## 9. Conclusion

In this paper we study theoretically the effect of a uniform long wave on a resonant triad of short gravity–capillary waves. To consider cases where the short-wave wavelengths are much smaller than the long-wave amplitude, we employ a Lagrangian formulation to simplify the description of the free surface. Without dissipation the equations governing the slow evolution of the wave envelope are derived for weakly nonlinear short waves on a gentle long wave. To the order of approximation dominated by quadratic interactions among the short waves, the long wave is shown to modify the evolution equation through terms with time-periodic coefficients. The interaction coefficients signifying the coupling between the short waves are found to be the same in both the Lagrangian and the Eulerian formulations. Important features of the nonlinear dynamics can therefore be expected to remain in either formulation. Detailed dynamics is then studied for the time evolution of short waves which are spatially uniform in a coordinate system moving with the long-wave flow. From the analytical solution without the long wave, bifurcations due to detuning have been examined. The bifurcation criterion of Chen & Saffman (1979) for collinear Wilton's ripples is found to apply to triads with arbitrary wavenumber configurations whenever the two longer waves have the same wave action. The effect of the long wave is then studied analytically for a weak disturbance. Modulational resonance of the short-wave envelope is studied when the long-wave frequency is a rational multiple of the natural modulational frequency of the triad. Several bifurcations of the Poincaré map are found, and confirmed by direct numerical integration. Finally, by increasing the amplitude of the long wave, Hamiltonian chaos is found to begin in two situations. The first one is due to the tangling of the homoclinic trajectory that can exist for a triad that is not disturbed by the long wave. The second one is due to the tangling of the homoclinic and heteroclinic manifolds of the Poincaré map associated with modulational resonance of the triad when it is disturbed by the long wave. It is found that when the two longer gravity–capillary waves have nearly the same wave action, then chaos is likely to be excited by the long wave provided the detuning from triad resonance is not large.

A number of theoretical questions remain, such as the concurrence of spatial and

temporal chaos, the effects of higher-order nonlinearity which may be important for longer time, the effect of damping and wind input, etc. More studies on these issues will help the understanding of the physical causes for randomness of the sea surface.

This research has been supported by the US Office of Naval Research Program on Ocean Engineering, Accelerated Research Initiative on Nonlinear Ocean Waves (grant N00014–92J–1754), the US National Science Foundation Program on Fluid Mechanics, Hydraulics and Particulate Systems (grant CTS–9115689), and the Norwegian Research Council for Science and the Humanities (grant NAVF 412.90/024) for a graduate fellowship (K. T.).

## Appendix. The governing equations

For this analysis it is sufficient to display linear and quadratic terms only. The continuity condition requires that the following expression is independent of time:

$$\frac{\partial x}{\partial a}+\frac{\partial y}{\partial b}+\frac{\partial z}{\partial c}-\frac{\partial x}{\partial b}\frac{\partial y}{\partial a}+\frac{\partial x}{\partial a}\frac{\partial y}{\partial b}-\frac{\partial x}{\partial c}\frac{\partial z}{\partial a}-\frac{\partial y}{\partial c}\frac{\partial z}{\partial b}+\frac{\partial x}{\partial a}\frac{\partial z}{\partial c}+\frac{\partial y}{\partial b}\frac{\partial z}{\partial c}. \tag{A 1}$$

Irrotationality, $x$-component:

$$-\frac{\partial^2 y}{\partial c\partial t}+\frac{\partial^2 z}{\partial b\partial t}+\frac{\partial x}{\partial c}\frac{\partial^2 y}{\partial a\partial t}+\frac{\partial^2 y}{\partial b\partial t}\frac{\partial y}{\partial c}-\frac{\partial x}{\partial a}\frac{\partial^2 y}{\partial c\partial t}-\frac{\partial y}{\partial b}\frac{\partial^2 y}{\partial c\partial t}$$
$$-\frac{\partial x}{\partial b}\frac{\partial^2 z}{\partial a\partial t}+\frac{\partial x}{\partial a}\frac{\partial^2 z}{\partial b\partial t}+\frac{\partial^2 z}{\partial b\partial t}\frac{\partial z}{\partial c}-\frac{\partial z}{\partial b}\frac{\partial^2 z}{\partial c\partial t}=0. \tag{A 2}$$

Irrotationality, $y$-component:

$$\frac{\partial^2 x}{\partial c\partial t}-\frac{\partial^2 z}{\partial a\partial t}-\frac{\partial^2 x}{\partial a\partial t}\frac{\partial x}{\partial c}+\frac{\partial x}{\partial a}\frac{\partial^2 x}{\partial c\partial t}+\frac{\partial^2 x}{\partial c\partial t}\frac{\partial y}{\partial b}-\frac{\partial^2 x}{\partial b\partial t}\frac{\partial y}{\partial c}$$
$$-\frac{\partial y}{\partial b}\frac{\partial^2 z}{\partial a\partial t}+\frac{\partial y}{\partial a}\frac{\partial^2 z}{\partial b\partial t}-\frac{\partial^2 z}{\partial a\partial t}\frac{\partial z}{\partial c}+\frac{\partial z}{\partial a}\frac{\partial^2 z}{\partial c\partial t}=0. \tag{A 3}$$

Free surface condition, $a$-component:

$$\frac{\partial^2 x}{\partial t^2}+g\frac{\partial z}{\partial a}+\frac{\partial x}{\partial a}\frac{\partial^2 x}{\partial t^2}+\frac{\partial y}{\partial a}\frac{\partial^2 y}{\partial t^2}+\frac{\partial z}{\partial a}\frac{\partial^2 z}{\partial t^2}+\gamma\left(-\frac{\partial^3 z}{\partial a\partial b^2}-\frac{\partial^3 z}{\partial a^3}\right.$$
$$+\frac{\partial^3 x}{\partial a\partial b^2}\frac{\partial z}{\partial a}+\frac{\partial^3 x}{\partial a^3}\frac{\partial z}{\partial a}+2\frac{\partial^2 x}{\partial a\partial b}\frac{\partial^2 z}{\partial a\partial b}+3\frac{\partial^2 y}{\partial a^2}\frac{\partial^2 z}{\partial a\partial b}+\frac{\partial^2 y}{\partial b^2}\frac{\partial^2 z}{\partial a\partial b}$$
$$+2\frac{\partial y}{\partial b}\frac{\partial^3 z}{\partial a\partial b^2}+3\frac{\partial^2 x}{\partial a^2}\frac{\partial^2 z}{\partial a^2}+\frac{\partial^2 x}{\partial b^2}\frac{\partial^2 z}{\partial a^2}+2\frac{\partial x}{\partial b}\frac{\partial^3 z}{\partial a^2\partial b}+2\frac{\partial y}{\partial a}\frac{\partial^3 z}{\partial a^2\partial b}$$
$$\left.+2\frac{\partial x}{\partial a}\frac{\partial^3 z}{\partial a^3}+\frac{\partial^3 y}{\partial a\partial b^2}\frac{\partial z}{\partial b}+\frac{\partial^3 y}{\partial a^3}\frac{\partial z}{\partial b}+2\frac{\partial^2 y}{\partial a\partial b}\frac{\partial^2 z}{\partial b^2}\right)=0. \tag{A 4}$$

Free surface condition, $b$-component:

$$\frac{\partial^2 y}{\partial t^2}+g\frac{\partial z}{\partial b}+\frac{\partial x}{\partial b}\frac{\partial^2 x}{\partial t^2}+\frac{\partial y}{\partial b}\frac{\partial^2 y}{\partial t^2}+\frac{\partial z}{\partial b}\frac{\partial^2 z}{\partial t^2}+\gamma\left(-\frac{\partial^3 z}{\partial a^2\partial b}-\frac{\partial^3 z}{\partial b^3}\right.$$
$$+\frac{\partial^3 x}{\partial a^2\partial b}\frac{\partial z}{\partial a}+\frac{\partial^3 x}{\partial b^3}\frac{\partial z}{\partial a}+\frac{\partial^2 x}{\partial a^2}\frac{\partial^2 z}{\partial a\partial b}+3\frac{\partial^2 x}{\partial b^2}\frac{\partial^2 z}{\partial a\partial b}+2\frac{\partial^2 y}{\partial a\partial b}\frac{\partial^2 z}{\partial a\partial b}$$

$$+2\frac{\partial x}{\partial b}\frac{\partial^3 z}{\partial a \partial b^2}+2\frac{\partial y}{\partial a}\frac{\partial^3 z}{\partial a \partial b^2}+2\frac{\partial^2 x}{\partial a \partial b}\frac{\partial^2 z}{\partial a^2}+2\frac{\partial x}{\partial a}\frac{\partial^3 z}{\partial a^2 \partial b}+\frac{\partial^3 y}{\partial a^2 \partial b}\frac{\partial z}{\partial b}$$

$$+\frac{\partial^3 y}{\partial b^3}\frac{\partial z}{\partial b}+\frac{\partial^2 y}{\partial a^2}\frac{\partial^2 z}{\partial b^2}+3\frac{\partial^2 y}{\partial b^2}\frac{\partial^2 z}{\partial b^2}+2\frac{\partial y}{\partial b}\frac{\partial^3 z}{\partial b^3}\Big)=0. \tag{A 5}$$

These equations have been worked out with the help of the symbolic computation program MACSYMA.

## REFERENCES


BANERJEE, P. P. & KORPEL, A. 1982 Subharmonic generation by resonant three-wave interaction of deep-water capillary waves. *Phys. Fluids* **25**, 1938–1943.

CASE, K. M. & CHIU, S. C. 1977 Three-wave resonant interactions of gravity–capillary waves. *Phys. Fluids* **20**, 742–745.

CHEN, B. & SAFFMAN, P. G. 1979 Steady gravity–capillary waves in deep water — I. Weakly nonlinear waves. *Stud. Appl. Maths* **60**, 183–210.

CHRISTODOULIDES, P. & DIAS, F. 1994 Resonant capillary-gravity interfacial waves. *J. Fluid Mech.* **265**, 303–343.

CRAIK, A. D. D. 1985 *Wave Interactions and Fluid Flows.* Cambridge University Press.

CRAIK, A. D. D. 1986 Exact solutions of non-conservative equations for three-wave and second-harmonic resonance. *Proc. R. Soc. Lond.* A **406**, 1–12.

CRAIK, A. D. D. 1988 Interaction of a short-wave field with a dominant long wave in deep water: Derivation from Zakharov's spectral formulation. *J. Austral. Soc.* B **29**, 430–439.

GRADSHTEYN & RYZHIK 1980 *Table of Integrals, Series and Products.* Academic Press.

GRIMSHAW, R. 1988 The modulation of short gravity waves by long waves or currents. *J. Austral. Math. Soc.* B **29**, 410–429.

HARRISON, W. J. 1909 The influence of viscosity and capillarity on waves of finite amplitude. *Proc. Lond. Math. Soc.* 7, 107–121.

HASSELMANN, K. 1967 A criterion for nonlinear wave stability. *J. Fluid Mech.* **30**, 737–739.

HENDERSON, D. M. & HAMMACK, J. L. 1987 Experiments on ripple instabilities. Part 1. Resonant triads. *J. Fluid Mech.* **184**, 15–41.

HENDERSON, D. M. & HAMMACK, J. L. 1993 Resonant interactions among surface water waves. *Ann. Rev. Fluid Mech.* **25**, 55–97.

HENYEY, F. S., CREAMER, D. B., DYSTHE, K. B., SCHULT, R. L. & WRIGHT, J. A. 1988 The energy and action of small waves riding on large waves. *J. Fluid Mech.* **189**, 443–462.

JANSSEN, P. E. M. 1986 The period-doubling of gravity–capillary waves. *J. Fluid Mech.* **172**, 531–546.

JANSSEN, P. E. M. 1987 The initial evolution of gravity–capillary waves. *J. Fluid Mech.* **184**, 581–597.

JONES, M. C. W. 1992 Nonlinear stability of resonant capillary-gravity waves. *Wave Motion* **15**, 267–283.

KAUP, D. J. 1981 The solution of the general initial value problem for the full three dimensional three-wave resonant interaction. *Physica* **3D**, 374–395.

LONGUET-HIGGINS, M. S. 1987 The propagation of short surface waves on longer gravity waves. *J. Fluid Mech.* **177**, 293–306.

LONGUET-HIGGINS, M. S. & STEWART, R. W. 1960 Changes in the form of short gravity waves on long waves and tidal currents. *J. Fluid Mech.* **8**, 565–583.

MA, Y.-C. 1982 Weakly nonlinear steady gravity–capillary waves. *Phys. Fluids* **25**, 945–948.

MCGOLDRICK, L. F. 1965 Resonant interactions among capillary–gravity waves. *J. Fluid Mech.* **21**, 305–331.

MCGOLDRICK, L. F. 1970 An experiment on second-order capillary gravity resonant wave interactions. *J. Fluid Mech.* **40**, 251–271.

MEISS, J. D. & WATSON, K. M. 1978 Discussion of some weakly nonlinear systems in continuum mechanics. In *Topics in Nonlinear Dynamics* (ed. S. Jorna), Vol 46, pp. 296–323. American Institute of Physics.

NACIRI, M. & MEI, C. C. 1992 Evolution of a short surface wave on a very long surface wave of finite amplitude. *J. Fluid Mech.* **235**, 415–452.

PERLIN, M. & HAMMACK, J. L. 1991 Experiments on ripple instabilities. Part 3. Resonant quartets of the Benjamin–Feir type. *J. Fluid Mech.* **229**, 229–268.

PERLIN, M., HENDERSON, D. M. & HAMMACK, J. L. 1990 Experiments on ripple instabilities. Part 2. Selective amplification of resonant triads. *J. Fluid Mech.* **219**, 51–80.

PERLIN, M. & TING, C.-L. 1992 Steep gravity–capillary waves within the internal resonance regime. *Phys. Fluids* A **4**, 2466–2478.

PHILLIPS, O. M. 1960 On the dynamics of unsteady gravity waves of finite amplitude. Part 1. The elementary interactions. *J. Fluid Mech.* **9**, 193–217.

PHILLIPS, O. M. 1981 The dispersion of short wavelets in the presence of a dominant long wave. *J. Fluid Mech.* **107**, 465–485.

REEDER, J. & SHINBROT, M. 1981 On Wilton ripples, I: Formal derivation of the phenomenon. *Wave Motion* **3**, 115–135.

SHYU, J.-H. & PHILLIPS, O. M. 1990 The blockage of gravity and capillary waves by longer waves and currents. *J. Fluid Mech.* **217**, 115–141.

SIMMONS, W. F. 1969 A variational method for weak resonant wave interactions. *Proc. R. Soc. Lond.* A **309**, 551–575.

STRIZHKIN, I. I. & RALETNEV, V. I. 1986 Experimental studies of three- and four-wave resonant interactions of surface sea waves. *Izv. Atmos. Ocean. Phys.* **22**(4), 311–314.

VYSHKIND, S. Y. & RABINOVICH, M. I. 1976 The phase stochastization mechanism and the structure of wave turbulence in dissipative media. *Sov. Phys. JETP* **44**, 292–299.

WERSINGER, J.-M., FINN, J. M. & OTT, E. 1980 Bifurcation and "strange" behavior in instability saturation by nonlinear three-wave mode coupling. *Phys. Fluids* **23**, 1142–1154.

WILTON, J. R. 1915 On ripples. *Phil. Mag.* **29**, 688–700.

WOODRUFF, S. L. & MESSITER, A. F. 1994 A perturbation analysis of an interaction between long and short surface waves. *Stud. Appl. Maths* **92**, 159–189.

ZHANG, J. & MELVILLE, W. K. 1990 Evolution of weakly nonlinear short waves riding on long gravity waves. *J. Fluid Mech.* **214**, 321–346.

ZHANG, J. & MELVILLE, W. K. 1992 On the stability of weakly nonlinear short waves on finite-amplitude long gravity waves. *J. Fluid Mech.* **243**, 51–72.